AIMS Geosciences, 5(2): 273–302.
DOI: 10.3934/geosci.2019.2.273
Received: 26 February 2019
Accepted: 21 May 2019
Published: 31 May 2019

http://www.aimspress.com/journal/geosciences

Research article

Geotechnical characterization of the Saint-Jude clay, Quebec, Canada

Ariane Locat[1,*], Pascal Locat[2], Hubert Michaud[2], Kevin Hébert[1], Serge Leroueil[1] and Denis Demers[2]

[1] Département de génie civil et de génie des eaux, Université Laval, Québec, Qc, Canada
[2] Section des mouvements de terrain, Direction de la géotechnique et de la géologie, Ministère des Transports du Québec, Québec, Qc, Canada

*** Correspondence:** Email: ariane.locat@gci.ulaval.ca; Tel: +14186562992.

Abstract: On May 10th 2010, a landslide occurred along the Salvail River in the municipality of Saint-Jude, tragically killing the four members of a family. The Ministère des Transports du Québec in collaboration with Université Laval carried out a detailed investigation to characterize the soil involved in this landslide. The investigation included field observations, in situ testing, sampling using thin-wall tubes, as well as laboratory tests that enabled to obtain information on the stratigraphy of the deposit and the geotechnical, mineralogical, micro-fabric and physico-chemical properties of the soils involved in the landslide. The stratigraphy and geotechnical properties were found to be uniform around the landslide. The clayey deposit is composed of various minerals dominated by quartz and feldspar, with a clay fraction containing large amounts of illite (or mica-like minerals) and a flocculated fabric. The soil involved in the landslide consists mainly of sensitive grey clay, typical of Canadian Champlain Sea clays, with a liquidity index varying between 2 and 1 from top to bottom of the deposit, intact shear strength increasing linearly with depth from 25 to 65 kPa, and an OCR decreasing with depth from 1.9 to 1.2. High quality samples were also taken using the Laval sampler. Triaxial tests were performed on these samples to characterized the mechanical behaviour of the Saint-Jude clay and its critical and limit states. The critical state is defined by a friction angle in the normally consolidation range of 30.6° and a cohesion of 5 kPa. The limit state is centered around the normally consolidated coefficient of earth pressure at rest line, with a peak strength envelope beyond the critical state envelope and an isotropic limit state equal to $0.7\sigma'_p$, typical for Champlain Sea deposits.

Keywords: sensitive Canadian clay; geotechnical properties; mineralogy; micro-fabric; limit state; landslide; spread

1. Introduction

On May 10th 2010, in the municipality of Saint-Jude located about 50 km northeast of Montréal, Canada (see Figure 1), a landslide, with an estimated area of 53,500 m^2, occurred and destroyed a house, killing its four inhabitants [1,2]. The debris was constituted of blocks having horst and graben shapes, typical of spreads in these clays. Given the particular nature of this landslide and its consequences, the Ministère des Transports du Québec (MTQ), in collaboration with Université Laval, carried out a detailed investigation in order to determine the characteristics and properties of the soil involved in this landslide. This investigation gives valuable and detailed information on a Canadian sensitive clay, prone to large landslides, that still remains a challenge for geotechnical engineers to work with.

The investigation included field observations, in situ testing, sampling using thin-wall tubes and Laval sampler [3], as well as laboratory tests that enabled to obtain information on the stratigraphy of the deposit and the geotechnical, mineralogical, micro-fabric and physico-chemical properties of the soils involved in the landslide. This paper describes the geology of the Saint-Jude area as well as the mineralogy and the micro-fabric of the sensitive clay deposit involved in the landslide along with its geotechnical and mechanical properties. The issue of spreads in these soils is also addressed by using the Saint-Jude case as an example.

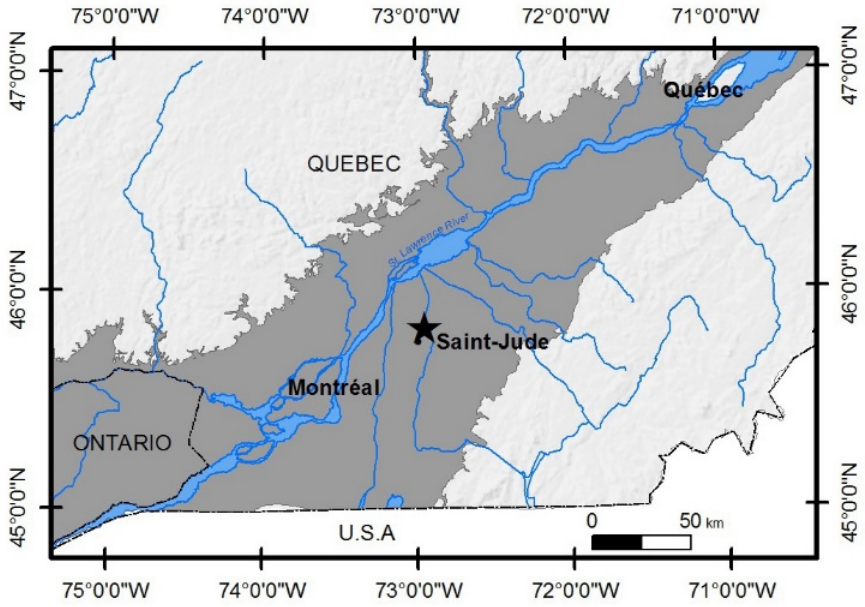

Figure 1. Location of the studied area (grey area shows the extent of the former Champlain Sea in this part of the St. Lawrence Valley) [1].

2. Geological context of the area

Figure 2 presents a digital terrain model of the area where the 2010 landslide occurred, its surroundings as well as the nearby Salvail and Yamaska Rivers. The morphology of the area is characterized by flat terrain, generally located at elevations lower than 100 m, in which rivers have carved valleys following the retreat of the Champlain sea about 10,000 years ago [4].

Globensky [5] describes the bedrock in this area as red shale and green sandstone from the Queenstone group of the Bécancour Formation, dating back to the Upper Ordovician (~450 Mya before present, BP.). Bedrock elevation in the area of the Saint-Jude landslide varies between −15 m to 5 m and comes up at about an elevation of 20 m East of the Yamasaka River. It forms a valley, shaped by glacial erosion, located underneath the Salvail River. This shape induces a variation in overlaying sediment thickness and locally favors the presence of artesian water pressure condition.

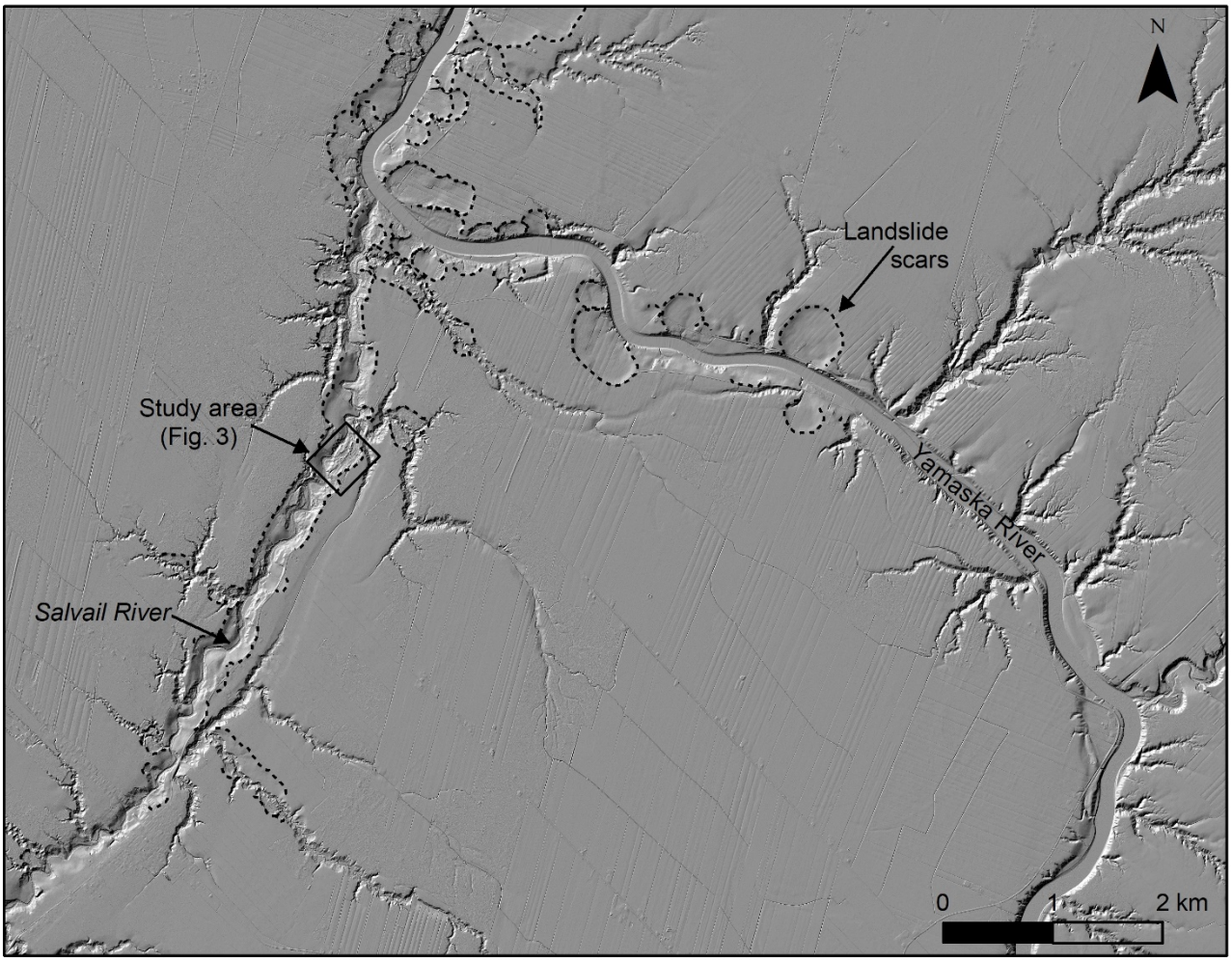

Figure 2. Digital terrain model of the study area.

The general stratigraphy of the Quaternary deposit overlying the bedrock is mostly uniform across the area and has been divided in five units by Rissmann et al. [6]. The first unit lying on the bedrock is a till, with a sandy matrix, having a thickness of no more than a few meters. A layer of sand and gravel of glacial origin and of variable thickness lies on top of the till. Above this unit, a deposit consisting of varved silty clay and fine sand is generally present in the area around the Yamaska River. This unit, which is not seen at the study area, has been associated to Glacial Lake Candona formed between the retreating Laurentide ice sheet and the Appalachian Mountains [7]. The northern end of that glacial lake would lie about 30 km to the south of the Saint-Jude Municipality which may explain why this unit is absent at the studied site. The following unit consists of a

stratified layer of marine and silty clay having a thickness that reaches up to 30 m. This layer is relatively uniform across the area and is associated with the former Champlain Sea that was formed as the glaciers retreated towards the North, about 12,000 years BP. [4]. The extent of the marine deposit of this former sea is shown in grey on Figure 1. This unit was deposited in deep to shallow marine environment having a salinity probably around 25 g/L [8]. With the retreat of the Champlain Sea and the transition to current conditions along the St. Lawrence River, a final thin layer of fluvial/alluvial sand, likely less than 10,000 years old, has been deposited which can be seen overlying the Champlain Sea unit.

The retreat of the glaciers was followed by an isostatic uplift of the area that was faster than the rise in sea level [4]. This brought the marine deposit in the area to elevations higher than the sea level and exposed it to fresh water [9]. The soils were therefore slowly leached and, in some areas, salt content became low enough for the clay to exhibit a high sensitivity. As can be seen on Figure 2, multiple landslide scars, of various sizes, shape the area, particularly along the Yamaska River. Some of these scars along the Salvail and Yamaska Rivers were made by retrogressive landslides, such as flowslides and spreads, and are indicators of the high sensitivity of the soil. This topography, with a typical dendritic drainage from river erosion, and this stratigraphy are typical of the Champlain Sea sediments in the region.

3. Investigation methods

The investigation following the 10th May 2010 aimed at studying the causes and characteristics of the landslide. It is described in detail by Locat et al. [2] and Locat et al. [1]. Work done at sites 32060, 32092, 32100, 32146, and 32230 to investigate intact soil and at 32103 in the debris (see locations in Figure 3) are described in this paper.

Table 1 describes the in situ tests and sampling methods carried out at each sites. Field investigation included cone penetration tests with pore pressure measurement (CPTU) at sites 32060, 32092 and 32100, giving detailed and continuous profiles of the corrected tip resistance (q_t), water pressure behind the cone (u2) and sleeve friction resistance (f_s), yielding precise information on the stratigraphic layers and their properties (adaptation of [10]). It has to be noted that CPTU at site 32060 was performed in 2004, six years before the landslide occurred, as part of a previous MTQ investigation regarding general geotechnical mapping in the area. In situ undrained shear strength was also obtained with field vane tests (S_{ufv}) carried out at sites 32092 and 32100 [11]. In situ pore water pressures (u_0) at different depths were measured with Casagrande type piezometers installed at sites 32100 and 32146. Samples were taken between depths of 2 m to 42 m at sites 32092 and 32100 using either a ~70 mm diameter and 600 mm in length thin-wall tubes, with no inside clearance, a cutting edge of 5 to 6°, and a Geonor fixed piston sampler for clay, or split-spoon sampler for stiff and coarse materials. Bedrock was found at a depth of 42.6 m at site 32100 and cored over a depth of 1.5 m. In 2015, during a later investigation focusing on the Saint-Jude clay mechanical behavior, 200 mm diameter and 660 mm in length high quality samples were taken with the Laval sampler [3] between depths of 8 and 12.2 m at site 32230.

Several of the thin-wall tubes and all the samples taken with the Laval sampler were examined with computerized axial tomography (CAT) scans to obtain detailed images of the stratigraphy of the samples.

The following standard geotechnical properties were obtained on soil specimens from the thin-wall tubes and the Laval sampler: particle-size distribution [12], water content [13], plastic limit (w_P [14]), liquid limit (w_L from Swedish fall cone [14]), intact ($S_{u\ cone}$) and remolded (S_{ur}) undrained shear strengths determined using the Swedish fall cone [15], preconsolidation pressure (σ'_p) from conventional incremental 24 hours oedometer tests [16] and hydraulic conductivity from laboratory falling-head permeability tests.

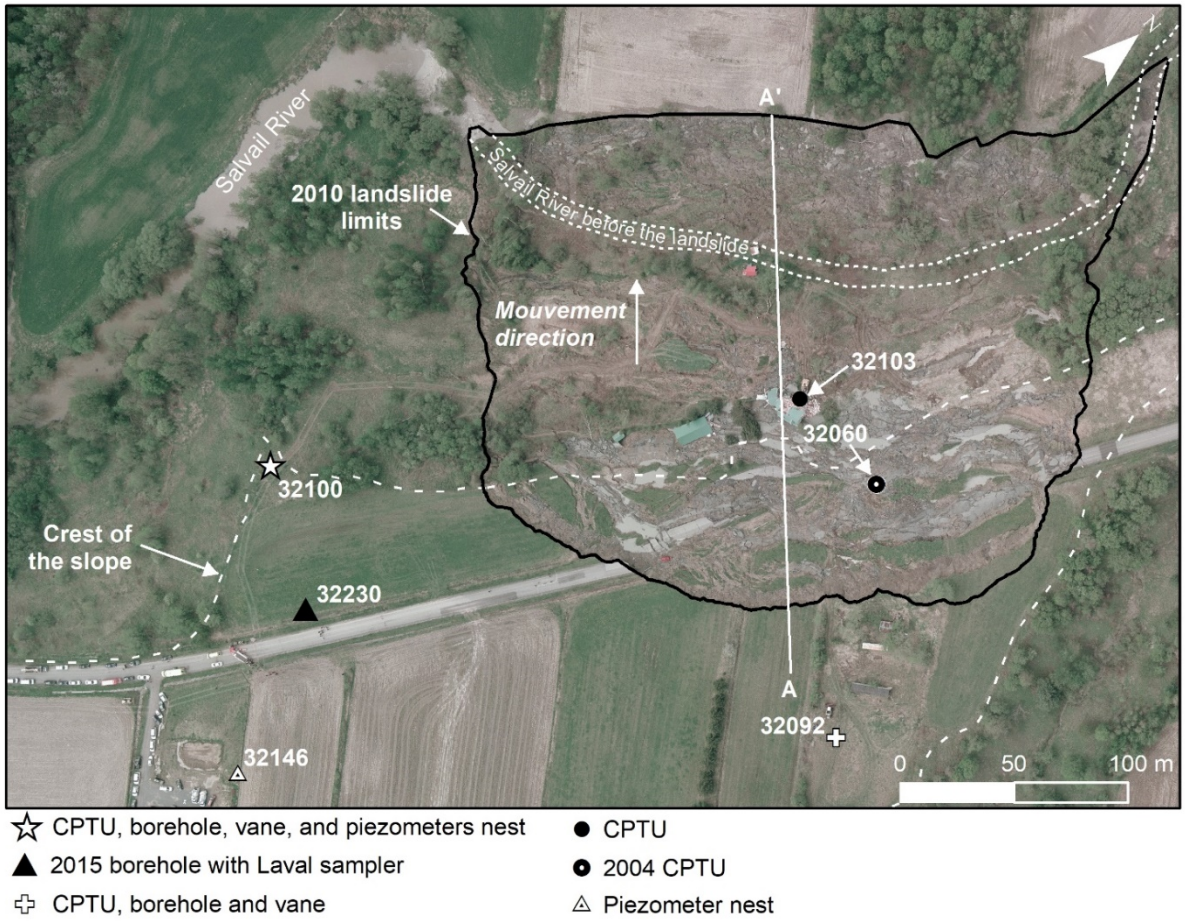

Figure 3. Boreholes and soundings locations selected for this study. Section A-A' is shown on Figure 19.

Table 1. In situ tests performed at each sites (see Figure 3 for location of these sites).

Sites	Date	CPTU	Field vane tests	Piezometers	Borehole with thin-wall tubes	Borehole with Laval sampler
32060	2004	X				
32092	2010	X	X		X	
32100	2010	X	X	X	X	
32146	2010			X		
32230	2015					X

X-ray diffraction of powder samples of the bulk specimen and of oriented samples of the clay fraction (CF), scanning electron microscope (SEM) observations and mercury intrusion porosity [17,18] were carried out on some samples to obtain information on the mineralogy and the micro-fabric of the soil. Specific surface area and cationic exchange capacity were also measured as well as organic matter, calcite content, and pore water salinity estimated from electric resistivity.

In addition, shear behavior of the soil involved in the landslide (peak shear strength envelope and limit and critical states) was studied with triaxial compression tests on samples taken with the Laval sampler. Ten samples were isotropically consolidated and sheared in undrained conditions (CIU), two samples were anisotropically consolidated and sheared in undrained conditions (CAU) and two samples were isotropically consolidated and sheared in drained conditions (CID). Axial deformation rate was of 0.0061 mm/min (~0.5%/h) for the undrained tests and 0.0012 mm/min (~0.1%/h) for the drained tests. The methodology used for processing triaxial data as well as the area and membrane corrections considered follows the one described by La Rochelle et al. [19] and ASTM Standards D4767-11 [20].

4. Composition, mineralogy and fabric

Combination of CPTUs, field vane tests and CPTUs at locations 32100, 32092 and 32230 with the laboratory tests enables to obtain information on the composition, mineralogy, fabric, state, index and engineering properties of the different clayey layers encountered on the study area. Information gathered at sites 32100 and 32230 is presented on Figure 4 and data from site 32092 is presented on Figure 5. Both profiles show similar information and, as only minor differences are observed on the elevation of the various units, description will follow profile 32100 (Figure 4) except for the top unit that was only sampled at site 32092 or when indicated otherwise.

4.1. Stratigraphy of the deposit

As shown on the geotechnical profiles (Figures 4 and 5), the deposit has been divided into five units (units A to E) who lie on the bedrock (unit R).

From the surface (elevation 28 m) to an elevation of 24.2 m, unit A is made of a dense, grey-brown, sandy fissured crust. This unit is composed of layers of sand and silt with only small amount of clay. Soil from this unit consists of 81% of silt (between 2 and 80 μm), 10% of clay (CF, < 2 μm), and 9% of sand (between 80 μm and 5 mm), see Figure 5.

From elevations 24.2 to 2 m, Unit B is composed of firm, grey, sensitive clay, very uniform with some silt. Photograph and CAT-scan image of a thin-wall tube sample from this unit is presented on Figure 6a. The clay is characterized by light and dark grey beds having a thickness of about 5 cm near the top of the unit, getting thinner than 2.5 cm near the bottom. The clay fraction is between 50% and 80%, silt fraction between 42% and 20% and sand fraction is lower than 2%. According to Rissmann et al. [6], this unit corresponds to the sediment associated with the Champlain Sea and is the main layer involved in the 2010 landslide [1,2]. CPTUs performed along the River Salvail show that properties of this unit are generally uniform across the area covered by the Saint-Jude municipality.

Unit C is found from elevation 2 to elevation −3 m, and is a stiff, silty clay of low sensitivity that can be divided into four layers. From elevations 1.5 to 0 m a grey silty clay with darker grey clay

nodules and a few seashells is identified. In this layer, two pinkish silty clay layers, having thickness of about 8 and 19 cm each and darker grey nodules, are also found at elevations of 1.1 and 0.9 m (pinkish layers in Figures 4 and 5). See Figure 6b for a photograph and a CAT-scan image of these layers sampled at site 32092. A grey silty clay layer with dark black spots is observed from 0 m elevation to an elevation of −0.7 m (dark grey layer in Figures 4 and 5). Photograph and CAT-scan image of the layer are shown on Figure 6c. The clay fraction is around 54%, silt fraction about 42%, and sand fraction lower than 3% through unit C. At the bottom of unit C, a grey silt and clay layer having thin sand and silt beds with a few seashells is observed. 1% of gravel (between 5 and 80 mm) is found near the bottom of the unit. This unit could correspond to sediments from the early Champlain Sea, as mentioned by Rissmann et al. [6], and would have formed just at the beginning of the sedimentary basin formation. At this time, this unit is interpreted as representing a debrite originating from a catastrophic event which occurred either within the Champlain Sea basin or from neighboring major rivers [8].

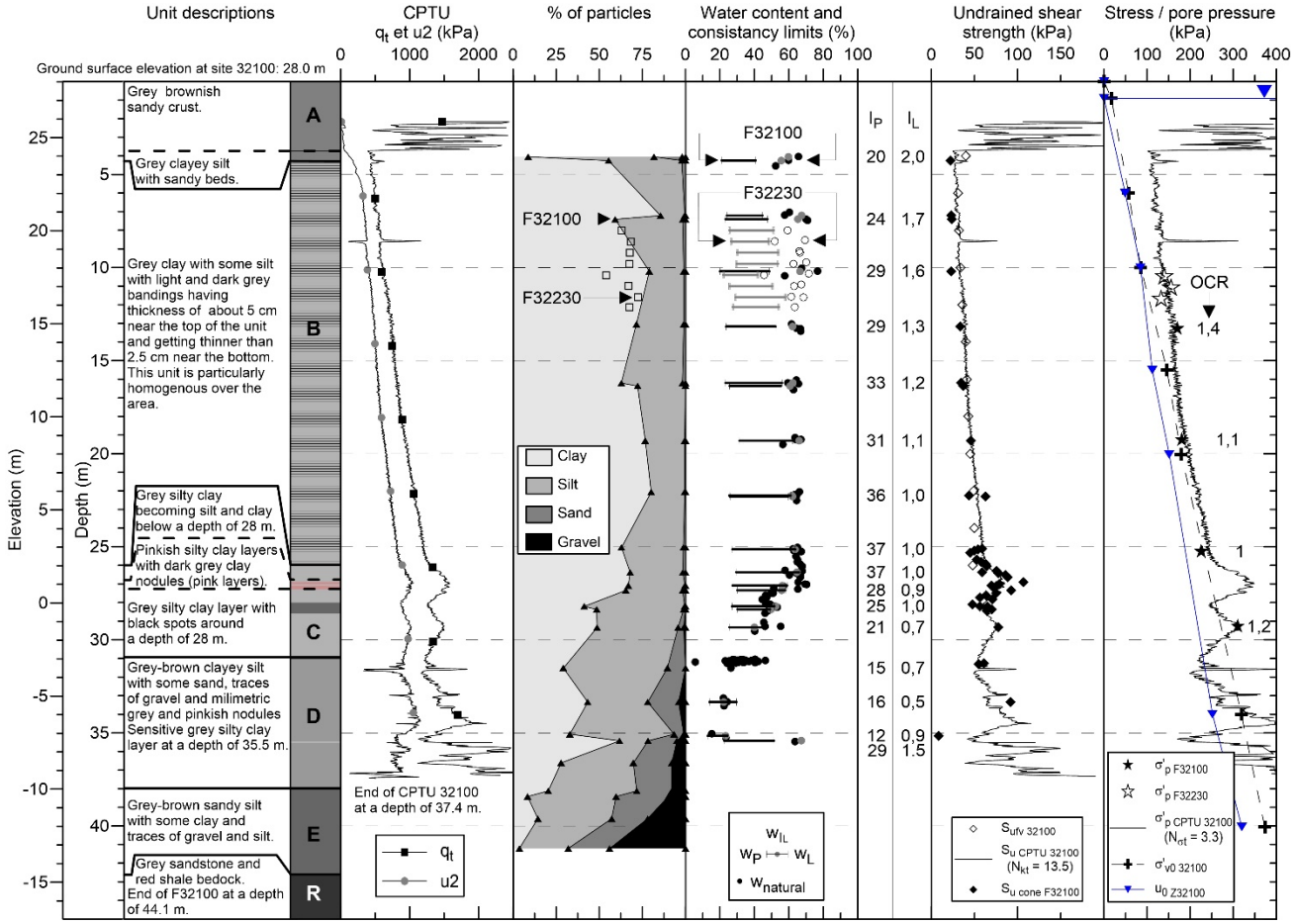

Figure 4. Geotechnical profile at sites 32100 and 32230 (see Figure 3 for location, modified from Locat et al. [2]).

From elevation −3 to −9 m unit D can be observed and is made of a very stiff, grey-brown clayey silt with gravel traces, becoming more sandy with depth. Photograph and CAT-scan image of the layer are shown on Figure 6d. The clay fraction is around 33%, silt fraction is around 40%, sand

fraction is below 17% and gravel fraction is higher than 10%. Soil in this unit is getting coarser with depth. One very soft grey clay layer was sampled at site 32100 at an elevation of −7.5 m (see Figure 4). Unit D could mark the transition from a glacial (unit E below) to a marine environment (unit C).

From elevation −9 to −14.6 m, unit E is made of hard, grey-brown, sandy silt with some clay and traces of gravel. The clay fraction varies between 4% and 20%, silt fraction varies between 51 and 28%, sand fraction is 24% in average and gravel varies between 8 to 44%. This unit is interpreted as a till layer overlying the bedrock.

The bedrock (unit R) is found below elevation −14.6 m and is made of grey sandstone and red shale of the Bécancour Formation.

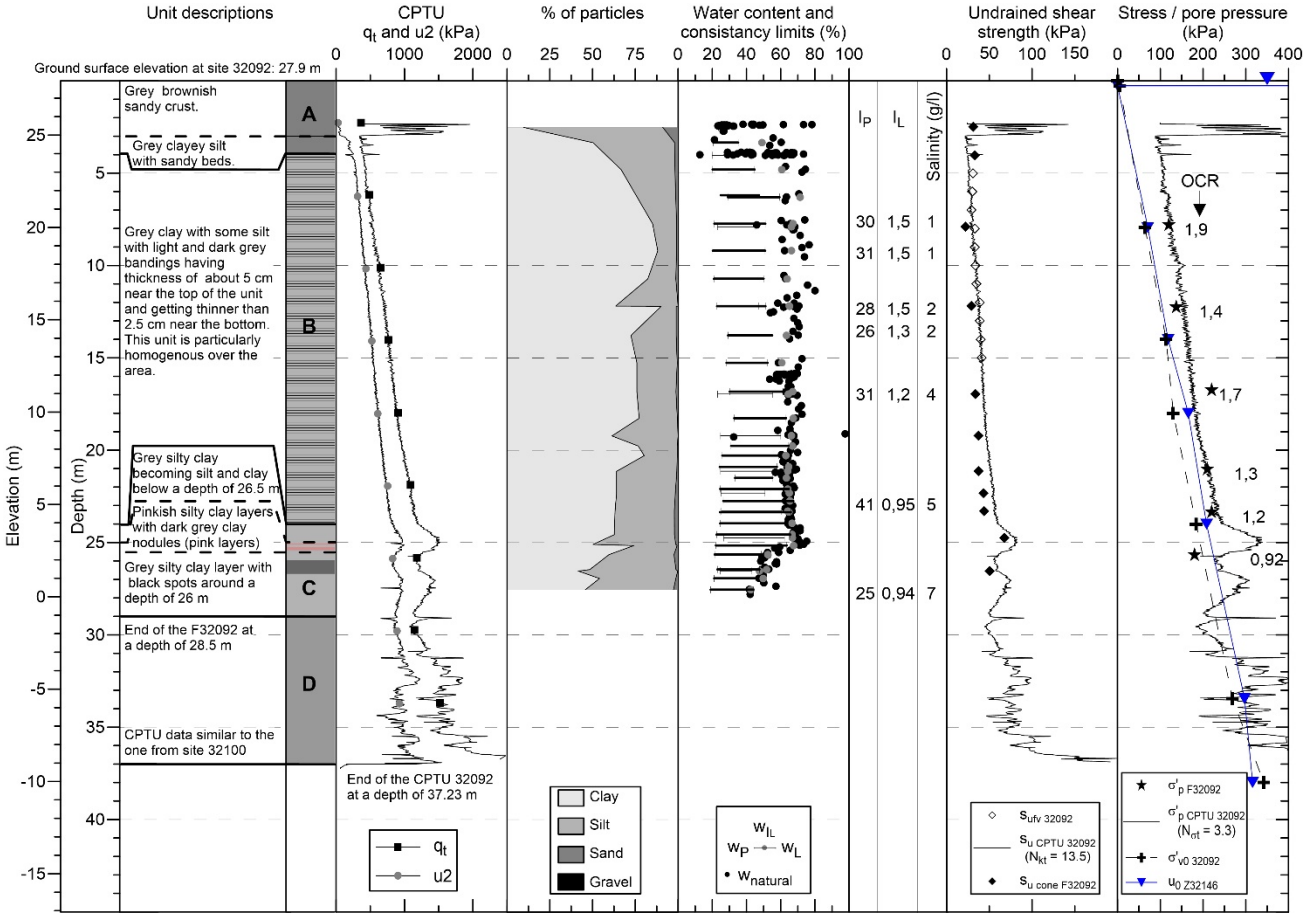

Figure 5. Geotechnical profile at site 32092 (see Figure 3 for location, modified from Locat et al. [2]).

4.2. Mineralogy and physico-chemical properties of the soil

Mineralogy, through X-ray diffraction, was studied on samples from unit B, taken at a depth of 19 m at site 32092 (elevation 8.9 m), and from the top grey layer in unit C, at a depth of 26.6 m at site 32100 (elevation 1.4 m). For simplification, depth will be used instead of elevation to locate samples. In addition, physico-chemical properties, such as organic matter (OM), calcite content ($CaCO_3$), specific surface area (SS) and cationic exchange capacity (CEC), were studied on these same samples as well as on samples from depths of 27.0 and 27.2 m (elevations 1 and 0.8 m) in the pinkish layers found in

unit C at site 32100, and in unit D taken at a depth of 31.3 m at site 32100 (elevation −3.3 m). The basic characteristics of the samples that were tested, such as clay fraction, water content (w), liquidity index (I_L) and plasticity index (I_P), are presented in Table 2 with a summary of these physico-chemical properties.

X-ray diffraction spectra obtained on powder samples from unit B and C are presented on Figure 7. Both spectra are similar, except for peak intensity, and show that both samples contain quartz (Qz), plagioclase feldspars (FaP), hornblende (Ho), potassium feldspar (FeK) and calcite (Ca). Illite (I) and chlorite (C) are also identified.

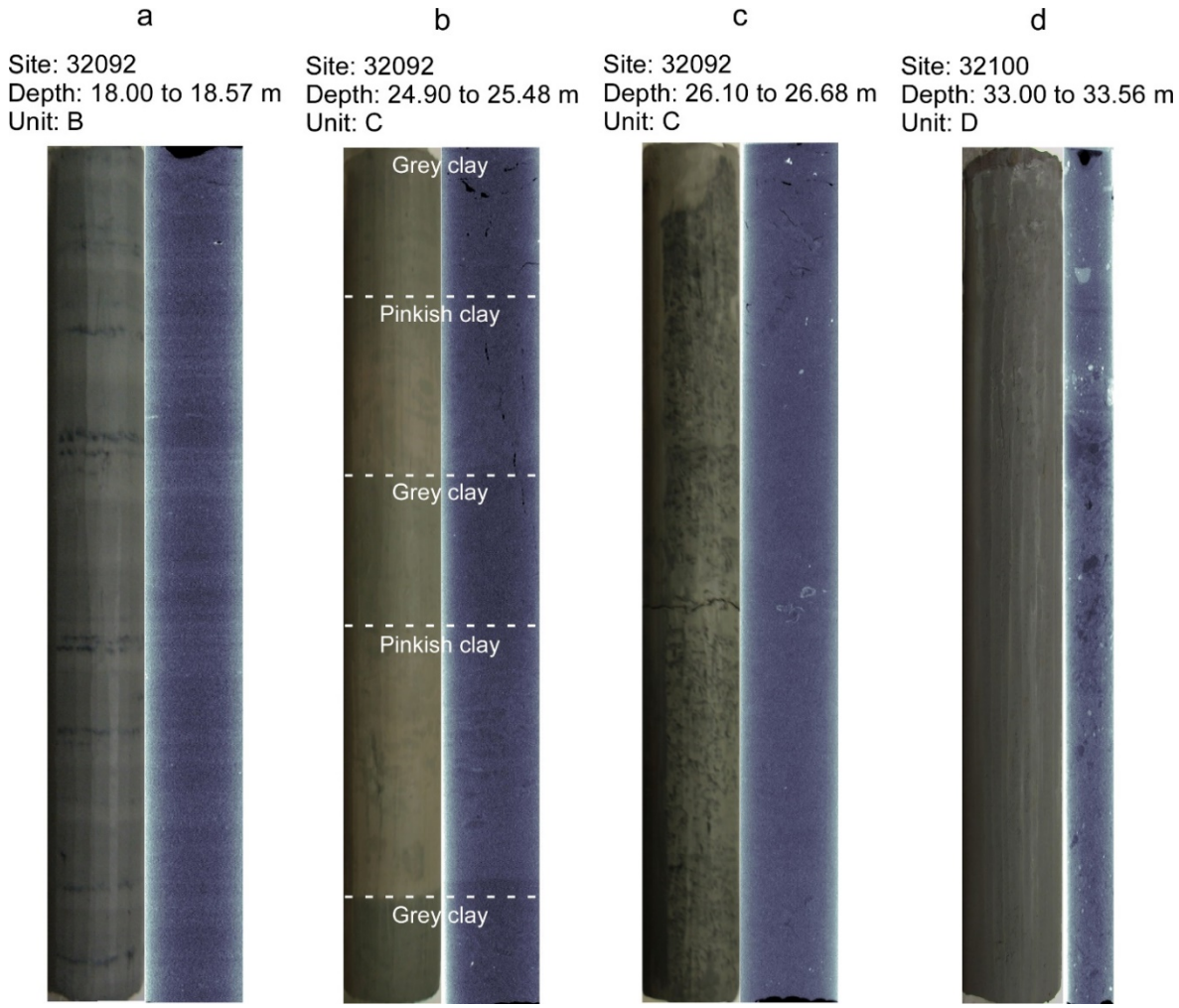

Figure 6. Photographs and CAT-scan images of samples from units B, C and D.

X-ray diffraction spectra of oriented clay fraction of samples from unit B and C are presented on Figures 8 and 9. These figures show the spectra for the natural clay fraction, after saturation with glycerol, and after heating up to 550 °C. Samples from unit B and C show similar results. Analysis of these spectra shows that the clay fraction of samples from both units contains illite, chlorite, kaolinite (Ka), and detectable amount of mixed-layers clay minerals or smectite (Sm), vermiculite (V) and hornblende. Peak at 7.5° (~12 Å) on the natural spectrum and more diffuse peak around 5° (~18Å) on the saturated glycerol spectrum show the presence of expandable clay mineral (mixed-layer mineral or smectite). These expandable clay minerals all contract upon heating to a value close to the

illite making the peak at about 8° significantly increase in height. The overall mineralogical composition of the St-Jude clay is quite typical for Champlain Sea sediments [21], that is, most of the soil originates from glacial erosion and is mainly constituted of rock flour.

Table 2. Physico-chemical properties of samples taken in units B, C, and D (see Figure 3 for location of these sites).

	Unit B	Unit C			Unit D
		Top grey layer	Pinkish layer	Pinkish layer	
Site	F32092		F32100		F32100
Depth (m)	19.0	26.6	27.0	27.2	31.3
Elevation (m)	8.9	1.4	1	0.8	−3.3
CF (%)[1]	62	68	67	65	29
w (%)	65.8	66.7	69.3	51.2	26.1
I_L[1]	1.2	1.0	0.9	0.9	0.7
I_P (%)[1]	35.2	36.6	31.7	27.9	15.4
OM (%)	0.7	0.6 and 0.7	0.3	0.4	0.4
$CaCO_3$ (%)	2.9 and 6.9	0.4 and 0.6	4.5	4.6	4.5
SS (m^2/g)	64	53 and 69	71	-	32
CEC (equ/100g)	10.5 and 11.2	10.8 and 11.3	9.6	8.8	3.5
Salinity (g/L)[2]	~4	~6	~6	~6	-
$A_c = I_P/CF$	0.6	0.5	0.5	0.4	0.5

[1] From sample nearby

[2] Interpolated from the salinity profile at site 32092 (Figure 5).

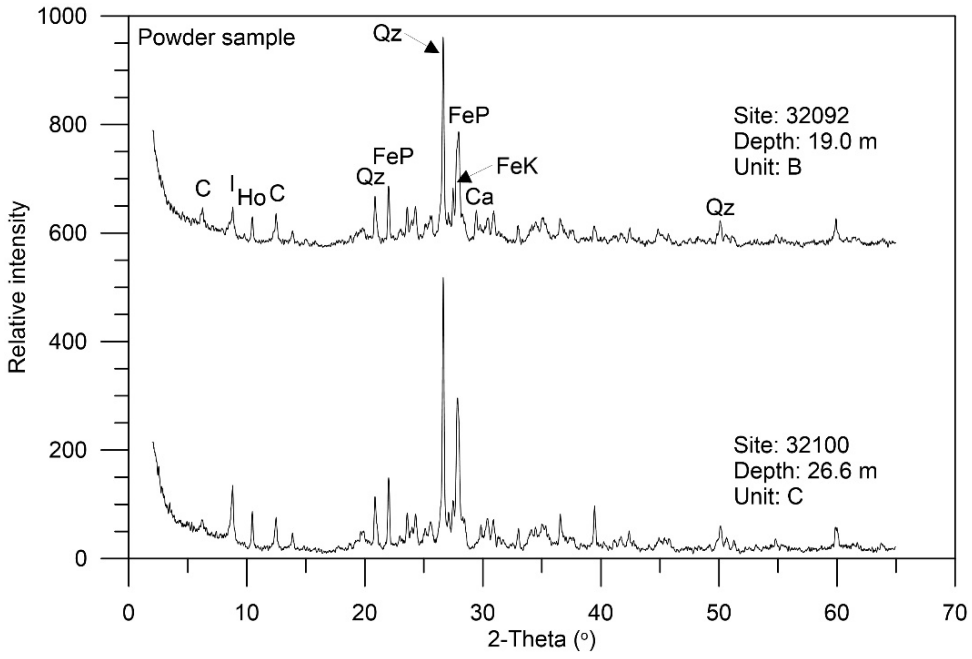

Figure 7. X-ray diffraction results on powder sample from units B and C.

Unit B has an organic matter content of 0.7% and calcite content varying between 2.9 and 6.9% (Table 2). Unit C top grey clay layer and lower pinkish layers have respectively organic matter content of about 0.7% (grey clay), 0.3% (top pinkish layer) and 0.4% (bottom pinkish layer). Calcite content is about 0.5% for the grey clay layer of unit C and around 4.5% for both pinkish layers. All the samples studied from unit C have a low organic content and the pinkish layers of unit C have more calcite than the upper grey one on the same unit. Unit D has organic matter and calcite content of 0.4 and 4.5%, respectively.

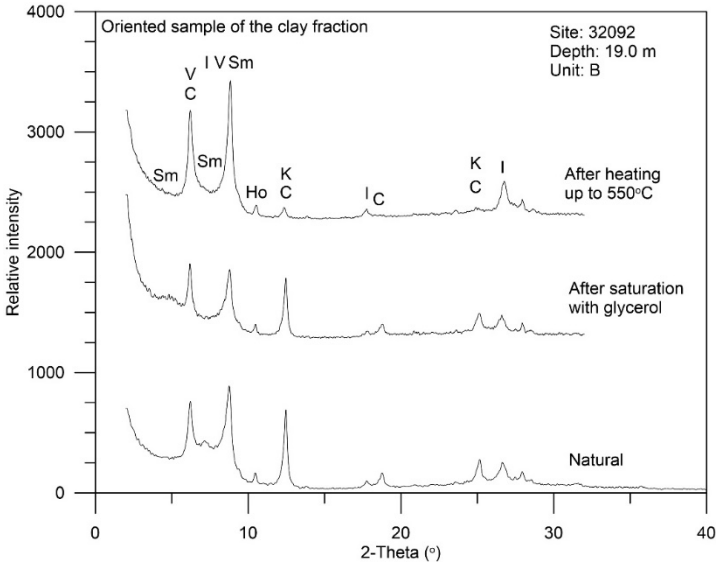

Figure 8. X-ray diffraction results on oriented sample of the clay fraction from unit B in its natural condition, after saturation with glycerol, and after heating up to 550 °C.

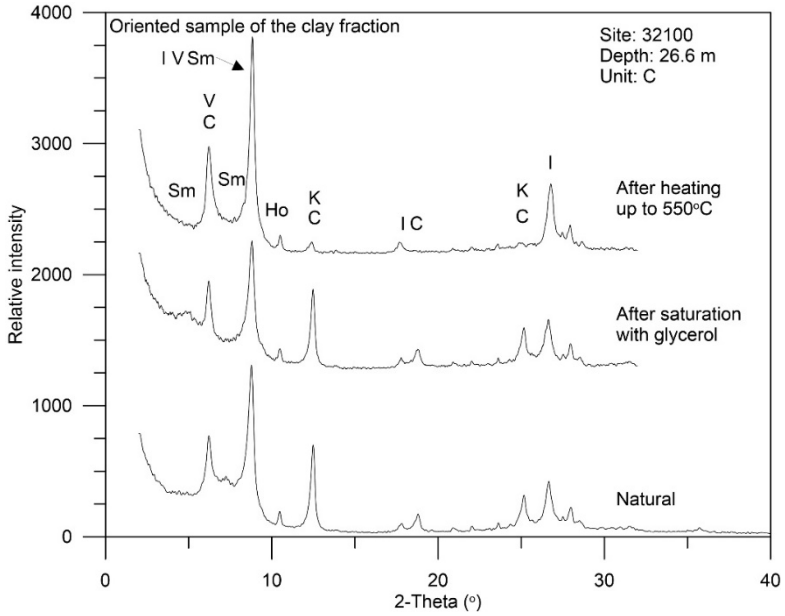

Figure 9. X-ray diffraction results on oriented sample of the clay fraction from unit C in its natural condition, after saturation with glycerol and, after heating up to 550 °C.

The specific surface area (SS) of the sample from unit B is 64 m^2/g. The grey clay at the top of unit C has a similar SS varying between 53 and 69 m^2/g and the one from the pinkish layers of unit C is 71 m^2/g (Table 2). Unit D has a SS of 32 m^2/g, the lowest of all sample tested.

Cation exchange capacity (CEC) of the sample from unit B varies between 10.5 and 11.2 equ/100g (Table 2). CEC from sample taken at the top of unit C (grey clay layer) is similar and varies from 10.8 and 11.3 equ/100g. CEC from samples taken in the pinkish layer of unit C are slightly lower and vary between 9.6 and 8.8 equ/100g. Unit D has the lowest CEC value of 3.5 equ/100g.

The salinity of the pore water was determined through electrical resistivity on samples taken at site 32092 at various depths (see Figure 5). It increases with depth from 1 g/L at 8 m (elevation 19.9 m) to 7 g/L at 28 m (elevation −0.1 m). From this profile, a salinity of 4 g/L and 6 g/L can be interpolated respectively for a depth of 19 m in unit B and for samples taken in unit C (see Table 2).

By dividing the plasticity index with the clay fraction (CF), the activity ($A_c = I_P/CF$) of the soil can be computed. (see Table 2). Activity of soil in unit B, of the top grey of unit C, of the pinkish clay of unit C and of unit D is respectively 0.6, 0.5, 0.5, 0.4, and 0.5. These values are similar, reflecting the consistent mineralogical nature of the soil.

These analyses indicate that soils sampled in unit B, C and D are inorganic with traces of calcite. Samples from unit B and C have mineral content similar to what has been observed in other areas in the Champlain Sea deposit with plagioclase being the most dominant mineral followed by illite and a few expendable clays as smectite and vermiculate [21]. SS and CEC are also in average of what has been observed for these soils in Québec. Soil from unit D, however, shows SS and CEC values in the lower range of what has been observed for eastern Canadian sensitive clays [21–23]. The increase in pore water salinity with depth would be consistent with a more pronounced leaching from the top of the deposit.

4.3. Fabric of the soil

Micro-fabric has been studied using scanning electron microscope (SEM) and mercury porosimetry on samples from unit B (depth of 18.9 m, elevation 9 m at site 32092) and the top grey layer in unit C (depth of 26.6 m, elevation 1.4 m at site 32100), very close to samples described in the previous section. Characteristics of these samples can therefore be found in Table 2. Specimens were prepared to analyse both vertical and horizontal planes.

Figures 10a–c present SEM photographs of the vertical plane of a sample from unit B magnified 500, 2000, and 5000 times. It can be seen that the sample is made of silt and clay particles smaller than 20 μm having angular, plate or foliated shapes. The fabric of the sample is homogenous and formed of many face-to-side contacts giving it a flocculated fabric. Particles seem to be slightly oriented with their long axis perpendicular to the maximum vertical stress axis. The fabric consists of aggregates and platy clay particles. Larger pores are found between flakes and between aggregates (inter-aggregate pores) and have diameters varying between 0.5 and 2 μm. The compaction of the soil makes it difficult to differentiate the flakes. The diameter of pores inside the flakes (pores intra-aggregates) are smaller than 0.25 μm. Looking at the vertical plane, the soil specimen from unit B is flocculated, compact with particles oriented according to the sedimentation. The horizontal plane (not presented here) shows more particle faces and less face-to-side contacts due to the orientation of the particles during sedimentation.

Figures 10d–f show SEM photographs of the vertical plane of a specimen from the top grey layer in unit C. Photographs show particles having angular, plate and foliated shapes with silt diameter or smaller. Two particles with diameter around 300 μm were also observed (not shown here). Micro-fossils are also found in the specimen. Some can be identified as diatoms, having diameters of 7 to 50 μm, and a foraminifera (not shown here) having a diameter of 300 μm. Broken micro-fossils seen in Figures 10 d,e,f are diatoms (made of silica). The sample shows several face-side contacts and a flocculated fabric. Due to a greater burial depth than the sample shown in Figures 10a–c, this sample presents a more compact fabric which makes it more difficult to evaluate the clay-flake orientation. On the other hand, the compaction from burial depth reached a point where most of the inter-aggregate pores are closed, while the intra-aggregate pores size has likely remained similar since their formation [17,18,24]. It is also interesting to note that at a magnification of 5000, large aggregates of particles (up to 10 μm in diameter) are visible just below the large diatom skeleton (at coordinate [6,16] in Figure 10f). One could think that these are already quite compact (i.e less compressible) and may be responsible for the apparent structuration effect resulting in a fairly constant water content (w) between depths of 5 m to 28 m (see Figures 4 and 5). As it will be shown in Section 6.3, such a structuration did not prevent the soil to be slightly overconsolidated in that unit. Intra-aggregate pores are smaller than 0.5 μm. Pores in open micro-fossils have diameter varying from 1 to 100 μm and limited preferential orientation, if one considers the broken diatoms. Pores inside micro-fossils skeletons shell are smaller than 0.5 μm. Horizontal plane (not shown here) shows similar observations with less face-to-side contacts.

Mercury porosimetry intrusion on samples from unit B at a depth of 18.9 m show that 0.697 and 0.789 mL of mercury was absorbed during the test, which corresponds relatively well with the water content of the sample (64.8%). Results also show a peak entry value of 0.2 μm followed by a constant value between 0.03 and 0.09 μm. These values could correspond respectively to inter-aggregates pore radius entrance and intra-aggregates pore radius entrance.

Mercury porosimetry on samples from the top grey layer of unit C at a depth of 26.6 m show that between 0.683 and 0.783 mL of mercury entered the samples during the test, corresponding well with the water content of the samples (65.1%). One peak entry value at 0.1 μ was detected, which corresponds to the average pore radius entrance of the samples, and is smaller than the pores observed with SEM and likely correspond to the intra-aggregate pores entrance.

It is to be noted that only few samples were tested to analyze the mineralogy and the physico-chemical properties of these units and that additional analyses are needed to make further conclusions.

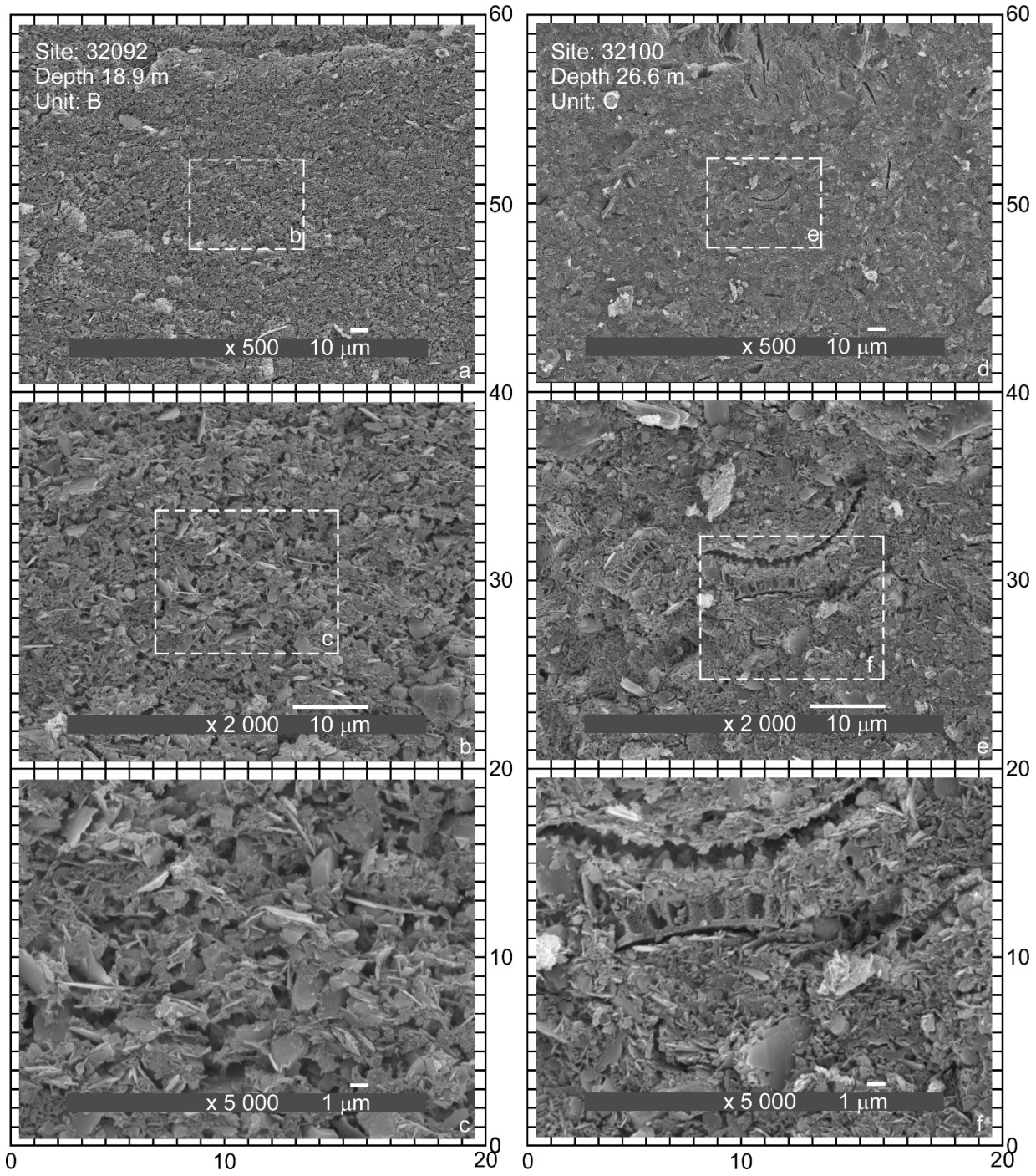

Figure 10. SEM photographs of samples from unit B and unit C showing the vertical plane (a and d) magnified 500 times, (b and e) 2000 times, and (c and f) 5000 times (White lines represent scale as indicated underneath).

5. State and index properties

Water content (w), liquid (w_L) and plastic (w_P) limits, as well as plasticity (I_P) and liquidity (I_L) indices from sites 32100, 32230, and 32092 are presented on Figures 4 and 5.

The water content in unit A, from elevation 28 to 24.2 m (elevation according to site 32100, Figure 4), varies between 24% and 78%.

From elevation 24.2 to 2 m, in unit B, the water content is about 65% over the entire unit, with a ±15% variability for the first 13 m and almost constant value below this depth. As soil in this layer is saturated, this indicates that the void ratio is also constant over the thickness of this unit, suggesting a possible structure/cementation in the clay that could have stopped the consolidation below a certain vertical stress level [25]. The plastic limit is fairly constant with depth in this unit and has a mean value of 26%. The liquid limit increases with depth from 45% to 65%. The salinity of the pore water varies from 1 g/L, at an elevation of 20 m, to 5 g/L, at an elevation of 5 m, and correlates well with the increase in liquid limit with depth. It can be seen that I_L decreases with depth from about 2.0 to 1.0 while the salinity increases.

In unit C, from elevation 2 to −3 m, the water content decreases with depth from 70% to 40%. The plastic limit decreases from 30% to 19% and the liquid limit from 64% to 46%. The liquidity index decreases from 1 to 0.7.

Water content in unit D is around 23%. The plastic and liquid limits are respectively 13% and 27%, giving a liquidity index of about 0.7.

6. Engineering properties of the Saint-Jude clay

6.1. Undrained shear strength

6.1.1. In situ intact undrained shear strength from field vane tests

Field vane tests were performed at sites 32100 and 32092 in unit B, results are shown on Figures 4 and 5. The intact field vane undrained shear strength (S_{ufv}) in unit B is 31 kPa at an elevation of 22 m and increase linearly to 48 kPa at elevation 2 m. The ratio between the vane shear strength and the preconsolidation pressure derived from conventional 24 hours oedometer tests (see sections 6.3) is 0.25 in average for both soil profile.

6.1.2. In situ intact undrained shear strength from CPTU results

CPTUs at sites 32092 and 32100 are presented on Figures 4 and 5 and detailed on Figure 11. They show the remarkable uniformity of the soil properties in the area. For simplification, the description herein will follow observations from site 32100 and will focus on unit B.

From an elevation of 24 m to an elevation of 2 m the corrected tip resistance (q_t) values increase linearly from 300 to 1400 kPa, while pore water pressure (u_2) and sleeve friction (f_s) increase respectively from 100 to 1000 kPa and from 1.5 to 20 kPa, denoting a fine-grained soil with a low permeability for unit B, the main layer involved in the 2010 landslide. Variations of f_s shown on Figure 11 are caused by the restarts of the CPTU driving during the test. The CPTU pore pressure parameter B_q ($B_q = (u2 - u_0)/(q_t - \sigma_{v0})$, were σ_{v0} is the in situ vertical total stress), shown on Figure 11, is around 0.7 in the clay layer (unit B) between 22 and −2.5 m of elevation. B_q between 0.42 and 0.82 are typical for Champlain Sea deposit [26].

Results from field vane tests were correlated with the CPTU net tip resistance ($q_t - \sigma_{v0}$) to obtain a dimensionless parameter for CPTU shear strength, $S_{u\ CPTU}$ ($N_{kt} = (q_t - \sigma_{v0})/S_{ufv}$),

estimated at 13.5. This N_{kt} value is consistent given the mean I_P of 26% of unit B and other values found in other Champlain Sea clay deposits [22,26]. The intact shear strength derived from CPTU ($S_{u\ CPTU}$) varies between 50 and 165 kPa for unit A. $S_{u\ CPTU}$ in unit B shows a linear increase from 25 to 65 kPa from the top to the bottom of unit B. $S_{u\ CPTU}$ throughout unit C is variable. It varies from 65 kPa at the top of the unit down to 50 kPa at the bottom of the unit with a peak of 86 kPa at an elevation of 1 m and another peak of 77 kPa at an elevation of −1.5 m. In unit D, $S_{u\ CPTU}$ varies between 50 and 150 kPa. It has to be noted that the N_{kt} value would be smaller if undrained shear strength from triaxial compression would have been used to correlate with the CPTU [27,28].

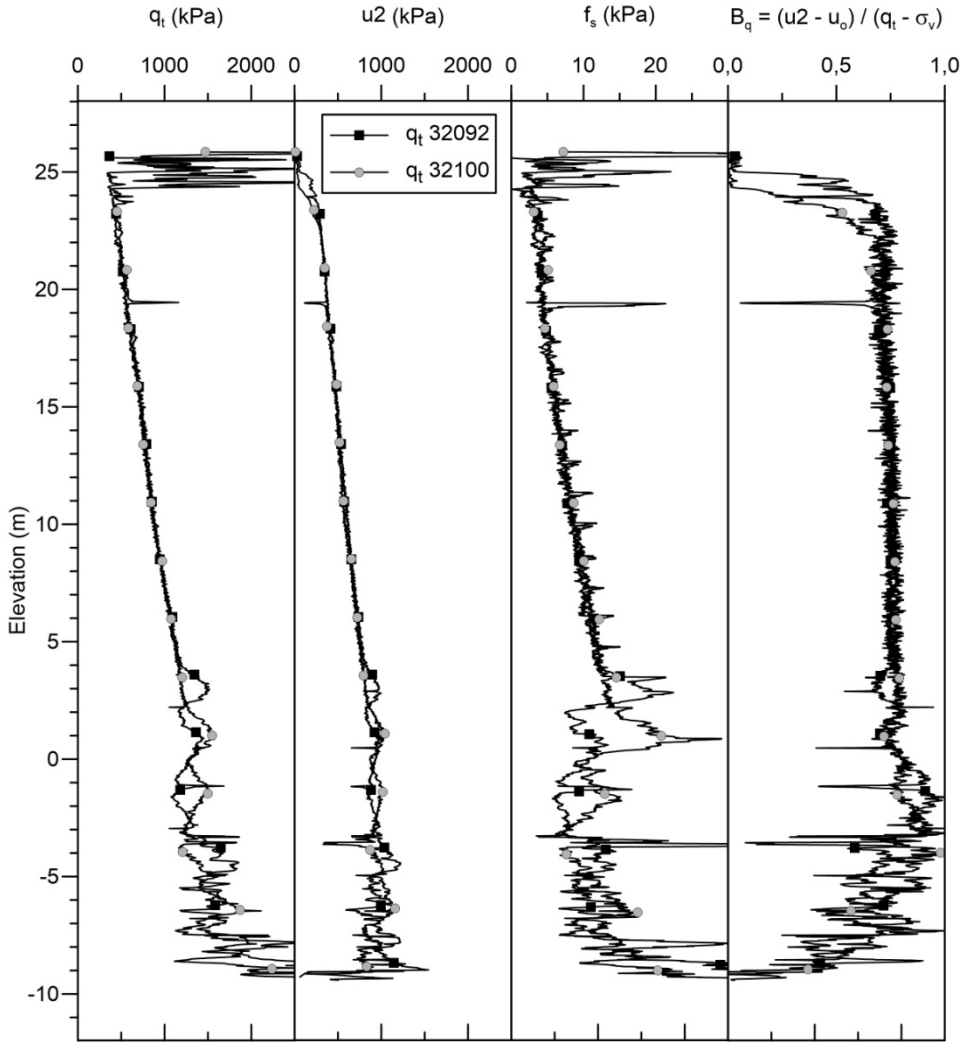

Figure 11. CPTU results at sites 32092 and 32100 (see Figure 3 for location of the CPTUs).

6.1.3. Triaxial undrained shear strength

Six undrained triaxial tests, for which specimens were consolidated under isotropical confining stresses varying between 30 and 91 kPa (CIU_{oc}), were carried out on samples taken between depths of 10.0 to 10.6 m in unit B with the 200 mm Laval sampler, at site 32230 (between elevations 18 and 17.4 m). These tests enabled to define the peak shear strength envelope in the overconsolidated range of the soil at this depth. Figure 12 presents the stress path of these tests in the Lamb diagram

($t = (\sigma'_1 - \sigma'_3)/2$ as a function of $s' = (\sigma'_1 + \sigma'_3)/2$, where σ'_1 and σ'_3 are the major and minor principal effective stresses respectively). It can be seen that all tests show a contractive stress-strain behavior, typical of sensitive Champlain clay [22] and that the peak shear strength envelope of this clay at this depth varies from 30 and 60 kPa for confining stress varying between 30 to 100 kPa. The undrained shear strength at a confining stress near the in situ effective stresses ($\sigma'_{v0} \approx 90$ kPa) is around 50 kPa, which is much larger than the in situ shear strength of 34 kPa from the field vane test at this depth (see Figure 4).

6.1.4. Fall cone shear strength and sensitivity

Fall cone intact shear strength ($S_{u\ cone}$), performed in unit B on samples from thin-wall tubes at site 32100 (Figure 4), is 22 kPa near the top of the unit and increases to 59 kPa near the bottom, following a similar trend then the S_{ufv} and $S_{u\ CPTU}$, with slightly lower values, as previously observed by Leroueil et al. [22]. Similar results are obtained at site 32092 (Figure 5).

Using Leroueil et al. [22] relationship linking I_L with remolded undrained shear strength (S_{ur}), S_{ur} varies from 0.3 to 1.6 kPa throughout unit B. Given the intact and remolded shear strengths, sensitivity varies from 80 to 40 from the top to the bottom of the unit. These sensitivity values are consistent with the pore water salinity profile and leaching from the top of the deposit.

Several fall cone tests on intact samples from unit C, at site 32100, were performed (Figure 4). $S_{u\ cone}$ values are around 51 kPa at elevation 2.8 m and around 60 kPa at elevation −0.3 m, with a maximum peak of 107 kPa at elevation 1.1 m and another one of 78 kPa at an elevation of −1.3 m. Shear strength obtained from fall cone tests follows similar trend as the one from the CPTU but shows a larger variability.

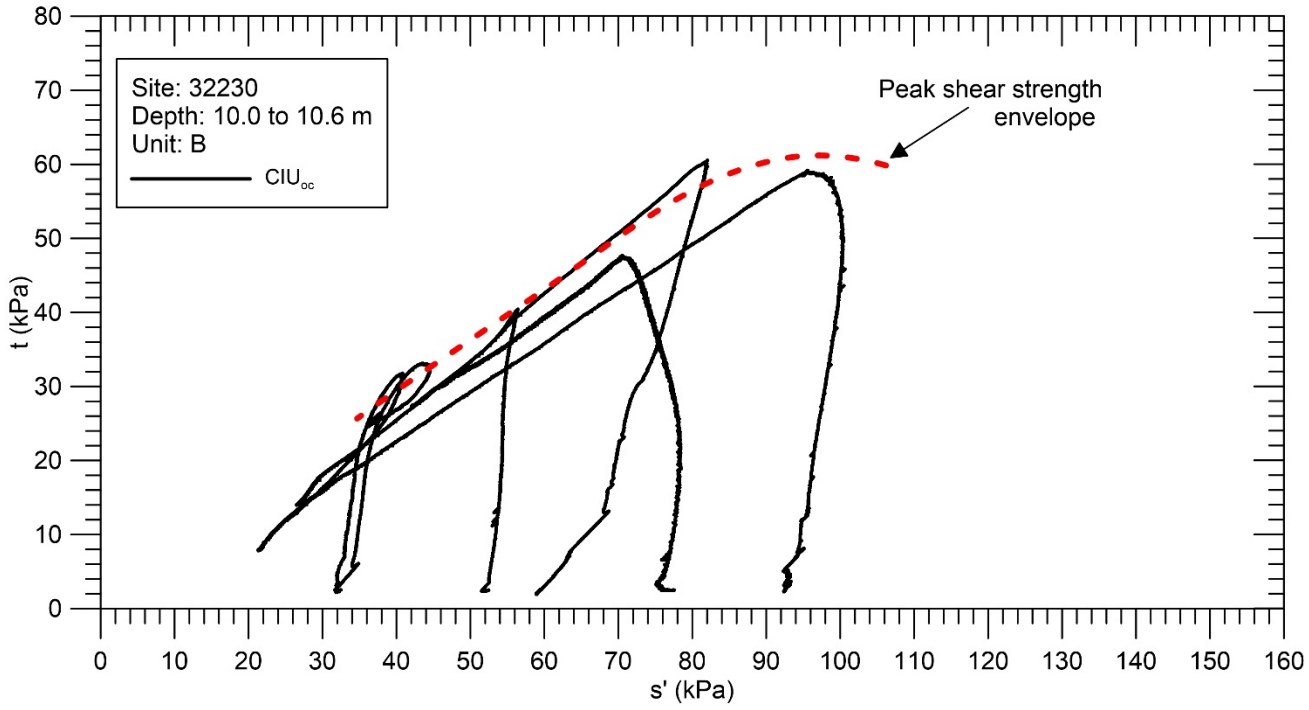

Figure 12. Peak shear strength envelope from undrained triaxial tests.

6.2. Oedometric compressibility

Three oedometer tests were performed on 200 mm diameter high quality Laval samples taken at site 32230, in unit B. These tests performed at depths of 10.5, 11.1 and 11.7 m are shown on Figure 13 (elevations of 17.5, 16.9 and 16.3 m). It can be observed that the preconsolidation pressure (from Casagrande construction) is well defined at values of 140, 156 and 132 kPa respectively for each depth. Maximal compression indexes (C_c) of 2.18, 1.72, and 1.94 are respectively obtained. C_c is maximal after the preconsolidation pressure and decreases at larger stress and lower void ratio. Given initial void ratios (e_0) of 1.79, 1.83, and 1.86 for each of the samples respectively, the C_c obtained from these tests follow correlations between e_0 and C_c for Champlain Sea clay discussed by Leroueil et al. [22]. Oedometers tests from ~70 mm diameter thin-wall tubes samples taken at various depth at sites 32100 and 32092 are also presented in Figures 4 and 5 and will be discussed in the following section.

6.3. In situ stress and OCR

In order to evaluate the in situ effective stress and the hydrogeological conditions of the deposit, piezometers were installed at site 32100. Six Casagrande type piezometers were installed at elevations of 22, 18, 12.5, 7.9, −6 and −12.1 m and an observation well was dug up from the surface. The latter enables to observe the elevation of the water table at a depth of 0.9 m (elevation 27.1 m). In situ pore water pressure (u_0) profile from piezometers at site 32100 is presented on Figure 4. Using piezometers at elevations 22 and 7.9 m, it is possible to measure a downward hydraulic gradient of 0.26 throughout unit B.

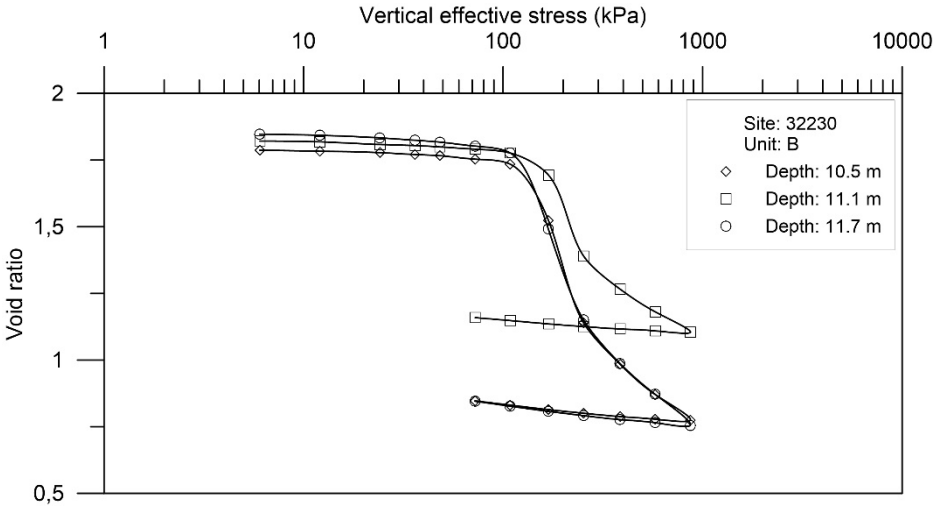

Figure 13. Oedometer tests results on samples from unit B at site 32230, taken with the Laval sampler.

Piezometers installed at site 32146 are considered representative of site 32092 and are used as estimates for the in situ pore water pressures at this site. Six Casagrande type piezometers and an observation well were put in place. Piezometers were installed at elevations of 19.9, 13.9, 9.9, 3.9, −5.6, and −10.1 m (these elevations are in reference to site 32092). The water table is observed at a

depth of 0.3 m (elevation 27.6 m) and the in situ water pressure profile obtained is shown on Figure 5. Using piezometers at elevations of 19.9 and 3.9 m in unit B, a downward hydraulic gradient of 0.13 is determined for this unit. This value is lower than the one measured at site 32100 and is in accordance with site 32146 being almost 100 m away from the crest of the slope (Figure 3).

To calculate the in situ total vertical stress on both sites, unit weight of 18.6, 16, 16.8, 19.3, and 20.7 kN/m^3 are assigned respectively to units A, B, C, D and E, in accordance with the average water content of these unit and specific density of 2.75 for the minerals. The calculated vertical effective stress (σ'_{v0}) profiles are shown in Figures 4 and 5.

Oedometer tests were performed on thin-wall tube samples from sites 32100 and 32092 and on high quality Laval samples from site 32230. Profiles of the preconsolidation pressure (σ'_p) are shown on Figures 4 and 5. Tests were mostly carried out on samples from unit B, but two tests were also performed on samples from unit C.

The preconsolidation pressure in unit B varies linearly from 120 kPa at an elevation of 20 m up to 220 kPa at an elevation of 5 m, giving overcosolidation ratios ($OCR = \sigma'_p/\sigma'_{v0}$) decreasing from 1.9 to 1.0 (see Figures 4 and 5). The clay in unit B is therefore lightly overconsolidated. As noted above, it is interesting here to remember that the water content profile does not seem to be strongly affected by the burial stress in that unit.

Preconsolidation pressure in unit C is equal to 180 kPa at an elevation of 2.2 m (depth of 25.7 m) at site 32092 (Figure 5) and to 310 kPa at an elevation of −1.3 m (depth of 29.3 m) at site 32100 (Figure 4), giving OCR of 0.9 and 1.2 respectively, thus close to 1.0.

Combining these preconsolidation pressures with the CPTU net tip resistance ($q_t - \sigma_{v0}$), a dimensionless parameter for CPTU preconsolidation pressure ($N_{\sigma t} = (q_t - \sigma_{v0})/\sigma'_p$) of 3.3 is obtained allowing to determine a preconsolidation from CPTU results ($\sigma'_{p\,CPTU}$). This $N_{\sigma t}$ value is in accordance with values obtained from other areas in Champlain Sea clay which have a typical value of 3.4 [26]. It can be said that the deposit is lightly overconsolidated, with a decrease in OCR with depth to a value close to 1.0 around elevation 3 m (depth of 25 m).

6.4. Hydraulic conductivity and void ratio relationship

Vertical hydraulic conductivity (k_v) was measured with falling-head permeability tests performed on thin-wall tube samples from a depth of 16.8 m in unit B (site 32092, elevation 11.1 m) and a depth of 33.3 m in unit D (site 32100, elevation −5.3 m) at five different void ratios (e) during incremental oedometer consolidation test. Hydraulic conductivity and void ratios relationship obtained from tests on soil from unit B is presented on Figure 14. For this specimen, a hydraulic conductivity of 9×10^{-10} m/s is measured at a void ratio close to initial void ratio (e_0), which is equal to 1.96 (k_{vA} on Figure 14). The relationship between void ratio and log k_v is linear with a permeability variation index ($C_k = \Delta e/\Delta log k_v$) close to 1. A hydraulic conductivity of 5.5×10^{-10} m/s is measured on the sample taken in unit D, having an e_0 of 0.72. A C_k value of 0.33 is found from the void ratio-logk_v relationship for this latter unit. Hydraulic conductivities obtained for both depths correspond to typical values obtained for Champlain Sea clay sediments and C_k values are in accordance with e_o of each sample [22].

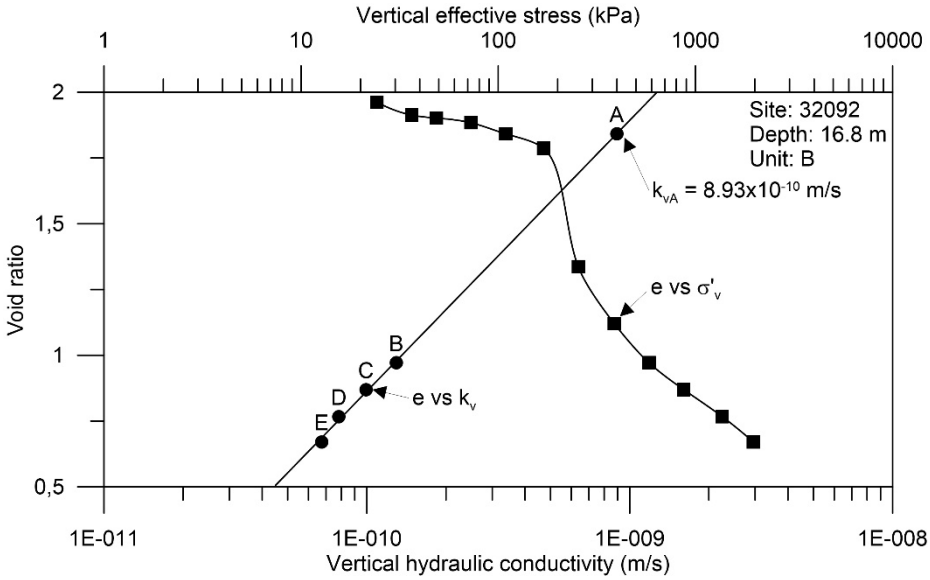

Figure 14. Void ratio-logk_v relationship obtained from falling-head permeability tests during incremental oedometer test on a sample from unit B.

6.5. Critical state and limit state surface of the Saint-Jude clay

Triaxial tests were carried out on Laval samples taken between depths of 10.0 to 10.6 m in unit B, at site 32230 (between elevations 18 and 17.4 m). Eight tests were isotropically consolidated to confining stresses between 30 and 91 kPa, in the overconsolidated range. These tests include six undrained tests (CIU_{oc}), mentioned above in section 6.1.3, and two drained tests (CID_{oc}). Two samples were also anisotropically consolidated with stress ratio (σ'_3/σ'_1) of 0.5 and 0.7 up to confining stress in the normally consolidated range of 135 and 150 kPa respectively and sheared in undrained conditions (CAU_{nc}). These tests were performed in order to characterize the limit state of this clay. Four additional tests were also performed in the normally consolidated range (CIU_{nc}, between confining stress of 195 and 400 kPa) in order to define the critical state line of the clay.

Figure 15a presents $t = (\sigma'_1 - \sigma'_3)/2$ as a function of the axial strain (ε_1). Figure 15b shows the shear induced pore water pressure during undrained shear (Δu, for CIU) and volume change during drained shear (ΔV, for CID) as a function of ε_1. Stress paths for all tests are shown in the Lamb diagram on Figure 15c (t as a function of $s' = (\sigma'_1 + \sigma'_3)/2$). It can be seen that the peak shear strength is reached at an axial strain below 1.5%, except for the CID tests where it is reached at an axial strain just above 2%. All tests show a contractive behavior with a peak shear strength and a lower large deformation shear strength typical of a strain-softening behavior.

The compression curves observed during the consolidation process of the triaxial CIU and CAU tests consolidated in the normally consolidated range are presented on Figure 16. It can be seen that the yield stress is well defined and reached at volumetric strain (ε_v) around 2%. Compression indexes (C_c) in the normally consolidated range vary between 1.2 and 1.6 for the CIUnc and are 1.8 and 2.9 for the CAUnc consolidated under anisotropic stress ratios respectively of 0.5 and 0.7.

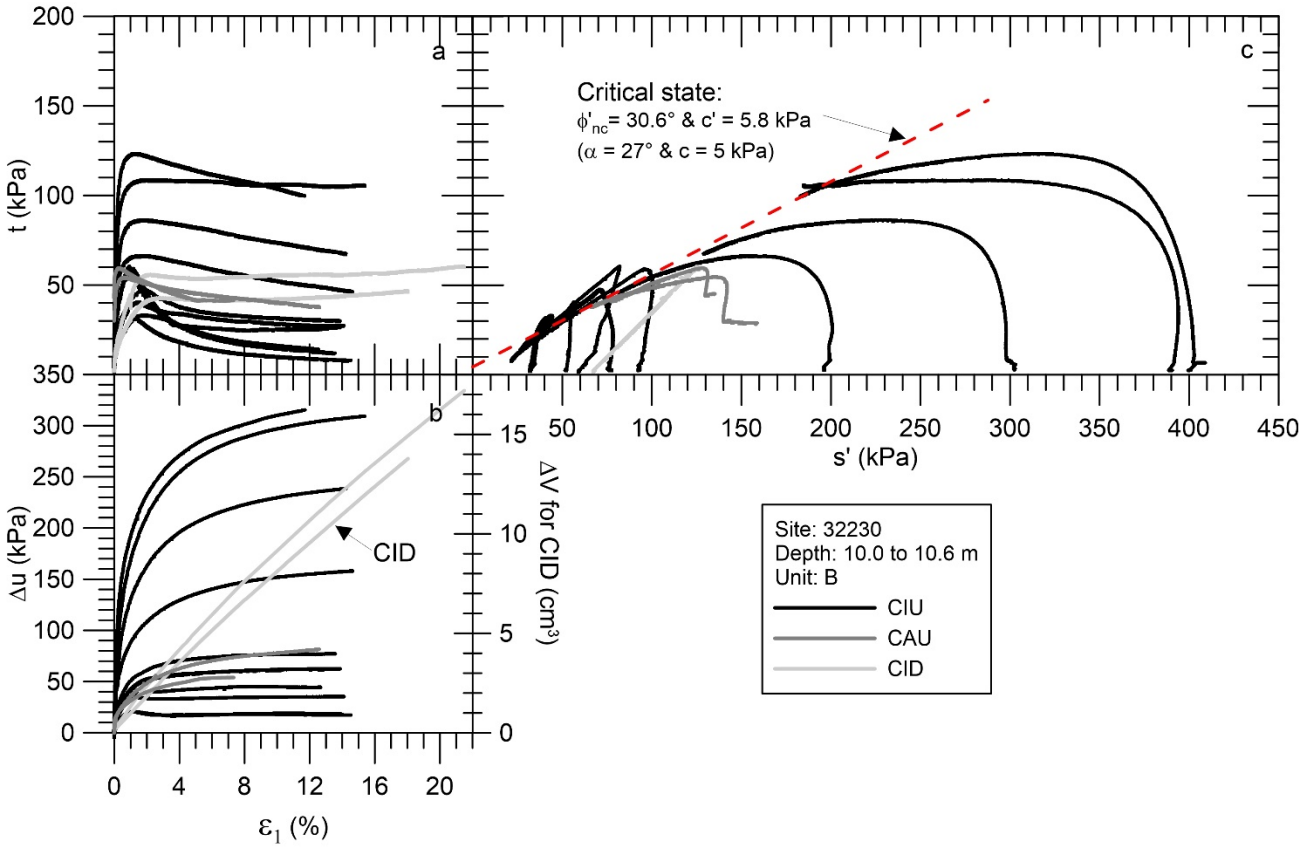

Figure 15. Results of CIU, CAU, and CID triaxial tests on samples from unit B taken with the Laval sampler.

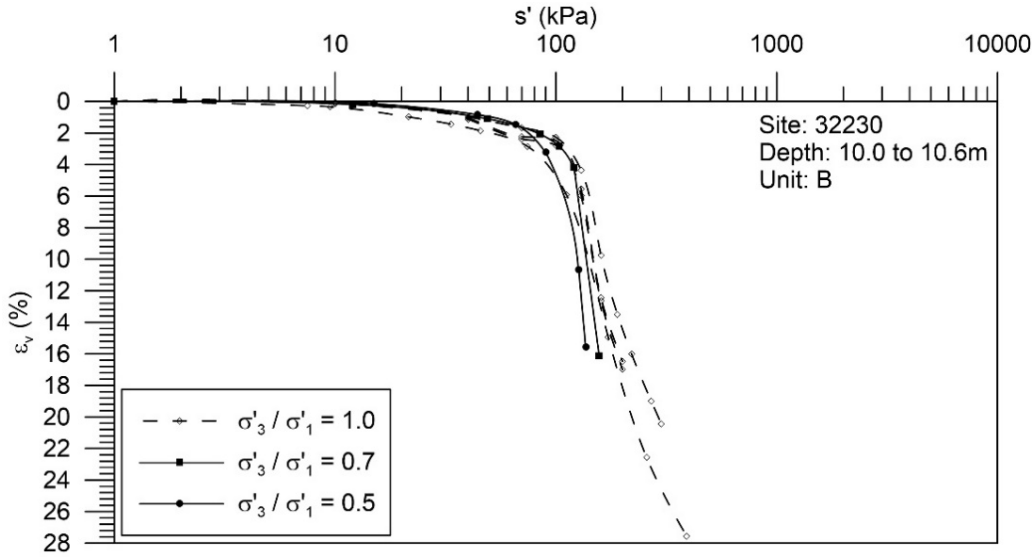

Figure 16. Compression curves of isotropic (CI) and anisotropic (CA) triaxial consolidation in the normally consolidated range on samples from unit B taken with the Laval sampler.

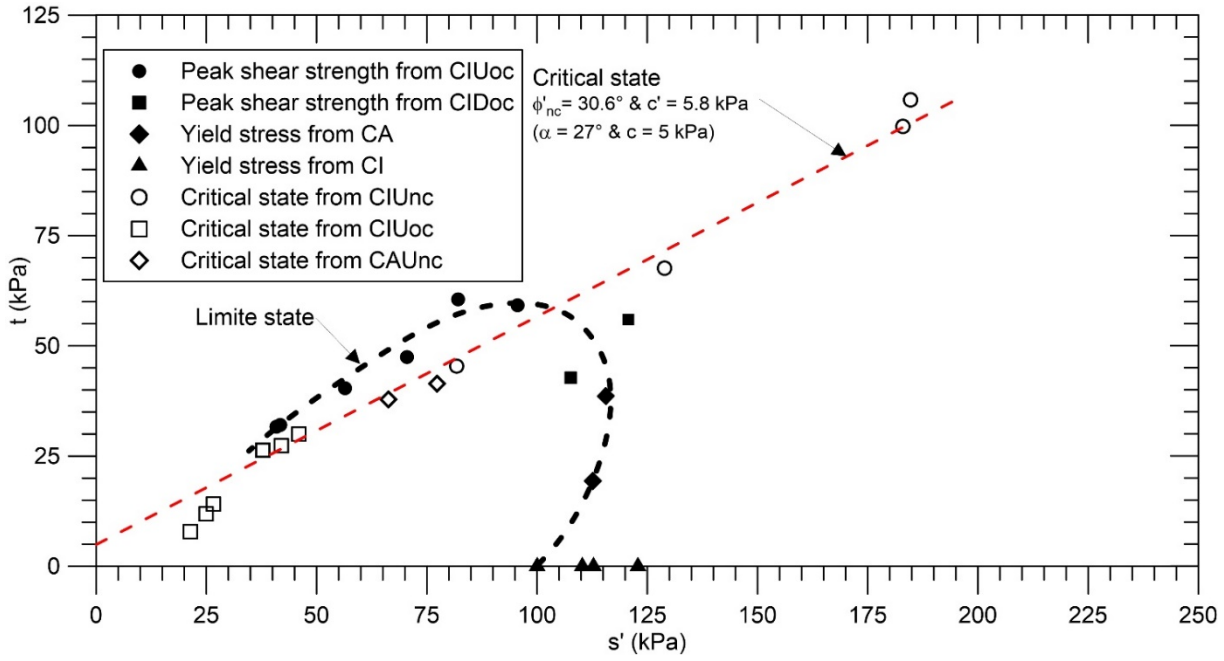

Figure 17. Limit state curve and critical state line for the Saint-Jude clay determined from tests shown on Figures 15 and 16.

Combining the last data points of the CIUnc tests (white circles on Figure 17) the critical state line was defined for the Saint-Jude clay (dashed red line). Effective friction angle (ϕ'_{nc}) and cohesion (c') are estimated at 30.6° and 5 kPa respectively. This ϕ'_{nc} value is consistent with the typical I_P of 29 at a depth around 10 m and is similar to other Champlain Sea clays having similar plasticity [22].

Peak shear strength of CIUoc (black circles on Figure 17) are used to determine the top of the limit state curve (dashed black line on Figure 17). Peak shear strength of the CIDoc tests are also used to determine the part of the limit state curve at larger stress, underneath the critical state (black squares on Figure 17), together with the yield points obtained from the anisotropic compression tests (CA, black diamonds) and isotropic compression tests (CI, black triangles). The limit state curve defined from these data points is shown with the dashed black line on Figure 17. It presents a peak strength envelope above the critical state line and is centered around the normally consolidated coefficient of earth pressure at rest line ($K_{0nc} = \sigma'_h/\sigma'_v$ of about 0.5, where σ'_{v0} and σ'_{h0} are the vertical and horizontal effective stresses respectively) of the clay. The general shape of the limit state curve is similar to those observed for other Champlain Sea clays. Using the preconsolidation pressure at a depth of 10.5 m at site 32230, estimated at 140 kPa (see Figures 4 and 14), the top of the limit state surface can be estimated at $0.4\sigma'_p$ and its boundary along the isotropic axis at about $0.7\sigma'_p$. Given the ϕ'_{nc} of 30.6°, these values would be in the upper range observed for Champlain Sea clay [22,29]. The data points used to define this limit state surface, however, show variability, mainly from yield points obtained from isotropic compression and from CID_{oc}.

7. Discussion on sample quality

LaRochelle and Lefebvre [30], Lefebvre and Poulin [31], La Rochelle et al. [3] and Leroueil et al. [22,32], discussed in detail how mechanical properties of Champlain clays are affected by

sampling disturbance. Lunne et al. [33] proposed the criteria described in Table 3 for evaluation of sample disturbance of marine clays with OCR between 1 and 2, using the normalized change in void ratio ($\Delta e/e_0$) when a sample is consolidated to the assumed in situ effective stresses. These criteria are used to assess quality of anisotropicaly consolidated samples compressed in the triaxial apparatus in undrained conditions (CAU). As indicated in Table 4, $\Delta e/e_0$ of 0.024 and 0.026 are obtained for the CAUnc tests. According to Lunne et al [33], such values below 0.04 indicate that these samples from the 200 mm diameter Laval sampler are of excellent quality, according to Lunne et al.'s criterion [33].

Table 3. Proposed criteria for evaluation of sample disturbance for OCR between 1 and 2.

Sample quality	$\Delta e/e_0$[1]
Very good to excellent (1)	0–0.04
Good to fair (2)	0.04–0.07
Poor (3)	0.07–0.14
Very poor (4)	> 0.14

[1] From Lunne et al. [33].

Lunne et al. [33] method can also be applied to the oedometer tests performed on Laval samples (see Table 4 and Figure 13). $\Delta e/e_0$ of 0.028, 0.026 and 0.042 are obtained at depths of 10.5, 11.1 and 11.7 m. These $\Delta e/e_0$ indicate that samples from depths of 10.5 and 11.1 m are of excellent quality and that the sample from 11.7 m is of good quality. The reason for this latter result showing, larger $\Delta e/e_0$, might however not be linked to sampling disturbance but to sample handling or to a poor contact with the sample at the beginning of the test.

Comparison with tests on samples taken with the thin-wall tubes is difficult, as no triaxial and oedometer tests were carried out on samples taken at similar depth with the thin-wall tubes at site 32100, the closest from site 32230.

Table 4. Sample quality assessment for tests on samples from site 32320.

Depth (m)	Sampler type	Test type	e_0	$\Delta e/e_0$
10.23	Laval	CAU_{nc} ($\sigma'_3/\sigma'_1 = 0.5$)	1.710	0.024
10.23	Laval	CAU_{nc} ($\sigma'_3/\sigma'_1 = 0.7$)	1.736	0.026
10.5	Laval	Oedometer	1.791	0.028
11.1	Laval	Oedometer	1.830	0.026
11.7	Laval	Oedometer	1.856	0.042

8. Engineering issues related to the Saint-Jude landslide

8.1. The 10th May 2010 landslide at Saint-Jude

The landslide occurred along the Salvail River, tragically killing a family of four as their residence was destroyed. A general view of the landslide is presented on Figure 18, showing the house and section of the road displaced by the ground movement. The area was thoroughly investigated after the landslide which occurred on May 10th 2010.

Figure 18. General view of the 10th May 2010 landslide at Saint-Jude.

Figure 19 presents a cross section showing the topography before and after the landslide. The landslide took place in a slope of 22 m in height and an inclination varying between 12 and 16°, with steeper parts having up to 20°.

The width of the landslide was 275 m, parallel to the river, and its length was 150 m perpendicular to the river. The retrogression distance, measured from the initial crest of the slope to the back scarp of the landslide was 80 m. The total area covered by the landslide and its debris is estimated at 53,500 m^2 and the total volume of the debris to about 520,000 m^3.

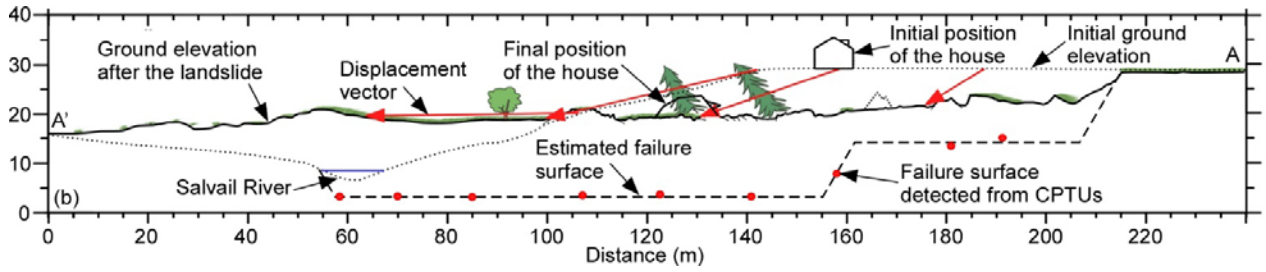

Figure 19. Cross section AA' (see Figure 3 for location of cross section).

As can be seen on Figures 18 and 19, the debris mainly stayed in the crater of the landslide, with little flow downstream in the river. It was mainly constituted of blocks of more or less remolded clay having graben and horst shapes, forming ridges inside the landslide scarp. Figure 20 shows a photograph of the debris of this landslide and an example of these blocks. Horsts are triangular blocks with tip pointing upward with horizontal stratification and grabens have flat horizontal surface covered with grass or trees, confirming that their movements are mostly horizontal. These debris are typical of spread, a landslide type that occurs in Eastern Canadian Sensitive clay [34–36].

Figure 20. Photograph of a horst, on the left with horizontal stratifications, and a graben on the right, covered with pieces of road and grass, in the debris of the Saint-Jude landslide.

The detailed 2010 investigation allowed to conclude that the soil involved in the landslide was mainly a firm, grey, sensitive clay, lightly overconsolidated, typical of the Champlain Sea sediments (unit B described above). The failure surface was identified by comparing CPTUs in intact soil to CPTUs inside the crater of the landslide, as showed on Figure 21. The failure surface is located at an elevation of 3.5 m, 2.5 m under the river bed elevation [1] (see red dots and dashed line on Figure 19). It is horizontal and continuous over a distance of about 115 m inside the deposit and then rises suddenly by about 10 m (to an elevation of 14 m) before reaching the back scarp of the landslide. This indicates that the failure surface has developed in two phases.

Given the high water head in the till layer (unit E described above), artesian conditions were observed in the till layer underneath the Salvail River [1,2] with a water head 12.5 m above the river level. In addition, erosion signs were observed on aerial photographs from before the landslide and seem to have contributed to decrease the stability of the slope with time. Considering the high water pressure, the analysis of the stability of the slope before the landslide showed that the safety factor for a first time failure was 0.99 in drained conditions [1,2]. The causes of the landslide are considered to be of natural origin and the stability of the initial slope decreased with time until a first failure occurred. It is not clear what was the importance of the magnitude of the trigger necessary to initiate this spread and the exact reasons explaining why a spread occurred at this location. However, it can be said that, as the safety factor of the initial slope was low, the magnitude of the trigger did not need to be large to initiate the main failure surface below the river bed.

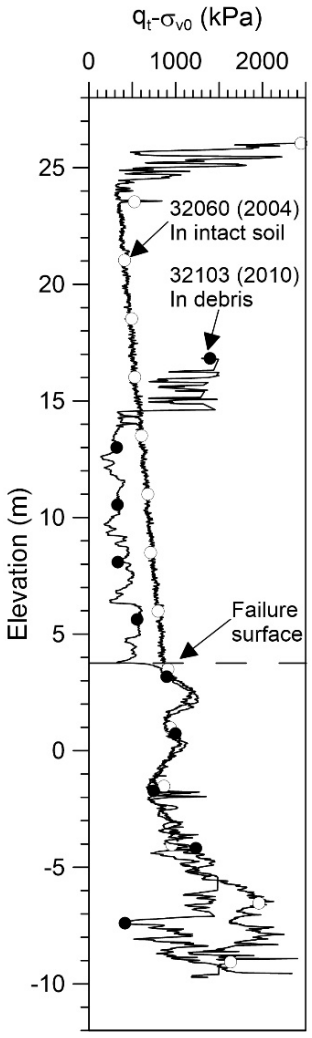

Figure 21. Location of the failure surface comparing net tip resistance from CPTU in intact soil (at site 32060) and in the debris (at site 32103). Note that CPTU at location 32060 was done in 2004, six years before the landslide (see Figure 3 for location of the CPTUs) [modified from 2].

8.2. Spreads in Canadian sensitive clays

According to Demers et al. [36], spreads constitute about 37% of large landslides inventoried in the past 100 years. 58% are flowslides and 5% are unidentified or from another type. When looking at the area where the 2010 Saint-Jude landslide occurred, as shown on Figure 2, it can be seen that various other landslides have happened in the past and that the 2010 event was not singular.

Unlike flowslides, appropriate conditions to initiate spreads have not yet been established. Analyses and compilation of several detailed cases of spreads [37] concluded that they can occur in slopes having various geometry and in clays having a large range of geotechnical properties and, in some cases, not sensitive enough to have flowslides (with liquidity index as low as 0.9). Previous studies [34,38–41] have mentioned how progressive failure, using the strain-softening stress-strain behavior of the soil, can explain the development of a quasi-horizontal failure surface, its progression into an intact soil mass, and the formation of a spread. Locat et al. [34,39,40] identified two distinct

processes associated with the occurrence of spreads in sensitive clay: (i) propagation of the failure surface horizontally into an intact soil mass and (ii) dislocation of the soil mass above the failure surface into horsts and grabens. These studies have shown the importance of analyzing the shear stresses on horizontal planes in the slope before these landslides, as they can be, in some cases, close to the peak shear strength of the soil and influence the stability of the slope. In addition, it was demonstrated that the post peak shear behavior of the soil has a major impact of the failure initiation and propagation. A better description of the brittleness and sensitivity of the soil and the shear band evolution along a failure surface during a landslide is therefore needed to improve our understanding of these events.

9. Conclusion

The paper has detailed the geological, geotechnical and mechanical properties of the clay at the 2010 Saint-Jude landslide area. The main unit involved in the landslide is a sensitive grey marine clay, deposited by the Champlain Sea clay. That sediment is composed of various minerals dominated by quartz and feldspar and with a clay fraction containing large amounts of illite (or mica-like minerals). The sediment has a flocculated microstructure. It is a firm clay with liquidity index varying from top to bottom of the deposit between 2 and 1, with an OCR decreasing from 1.9 to 1.2. The friction angle in the normally consolidation range is 30.6° and the limit state is centered around the K_{0nc} line, with a peak envelope beyond the critical state and an isotropic limit state equal to $0.7\sigma'_p$. Its characteristics are very uniform in the area of the landslide and typical of Champlain clays.

The intense field work carried out at Saint-Jude enabled a unique detailed description of the soil involved in a spread in sensitive clay. The investigation also reveals the complex nature of the failure surface development and the resulting dislocation of the failed mass into horsts and grabens. For all these reasons, the Saint-Jude landslide site is now a major reference site in Champlain Sea clays which will continue to be investigated in order to help understanding sensitive clays and mitigating large landslides such as spreads.

Acknowledgments

The authors would like to acknowledge the collaboration of the Saint-Jude municipality and the Saint-Jude citizens that was essential during the investigation. Sincere thanks also go to the family of the victims of this tragic event.

Genuine thanks to many people at the MTQ who contributed to this work: Martin D'Anjou, Thomas Fournier, Gilbert Grondin, Denis Hudon, Daniel Ouellet, Mélissa Raymond and Denis Robitaille.

The Ministère de la Sécurité Publique du Québec, the Fonds de recherche sur la nature et les technologies du Québec and the Natural Sciences and Engineering Research Council of Canada are also acknowledged for their financial contribution.

Professor Jacques Locat and the two reviewers of this paper are also acknowledged for their comments that contributed in improving this paper.

Conflict of interest

The authors declare no conflict of interest in this paper.

References

1. Locat A, Locat P, Demers D, et al. (2017) The Saint-Jude landslide of 10 may 2010, Quebec, Canada: Investigation and characterization of the landslide and its failure mechanism. *Can Geotech J* 54: 1357–1374.
2. Locat P, Fournier T, Robitaille D, et al. (2011) Glissement de terrain du 10 mai 2010, Saint-Jude, Montérégie, Rapport sur les caractéristiques et les causes. Rapport MT 11-01. Section des mouvements de terrain, Services de la géotechnique et de la géologie, Ministère des transports du Québec. Bibliothèque et Archives nationales du Québec, Gouvernement du Québec.
3. La Rochelle, Sarrailh J, Tavenas F, et al. (1981) Causes of sampling disturbance and design of a new sampler for sensitive soils. *Can Geotech J* 18: 52–66.
4. Gadd NR (1988) The late quaternary development of the Champlain sea basin. *Geol Surv Can*, 85–21.
5. Globensky Y (1987) *Géologie des Basses-Terres du Saint-Laurent*. Ministère de l'Énergie et des Ressources, Québec, Rapport MM85-02.
6. Rissmann P, Allard JD, Lebuis J (1985) Zones exposées aux mouvements de terrain le long de la rivière Yamaska, entre Yamaska et Saint-Hyacinthe, Ministère de l'Énergie et des Ressources, *Rapport DV* 83-04.
7. Parent M, Occhietti S (1999) Late wisconsinian deglaciation and glacial development in the Appalachians of southeastern Québec. *Géogr Phys Quat* 53: 117–135.
8. Cronin TM, Manley PL, Brachfeld S, et al. (2008) Impact of post-glacial lake drainage events and revised chronology of the Champlain Sea episode 13–9 ka. *Paleogeogr Paleoclimatology Paleoecol* 262: 46–60.
9. MacPherson JB (1967) Raised shorelines and drainage evolution in the Montréal Lowland. *Cah Géographie Québec* 11: 343–360.
10. ISO (2012) Reconnaissance des essais géotechniques—Essais en place. *ISO 22476-1*, 38.
11. ASTM (2018) Standard test method for field vane shear test in saturated fine-grained soils. *ASTM International*, West Conshohocken, PA, 8.
12. CAN/BNQ (2013) Sols-Analyse granulométrique des sols inorganiques. *BNQ 2501-025*, 34.
13. CAN/BNQ (2014) Sols-Détermination de la teneur en eau. *BNQ 2501-170*.
14. CAN/BNQ (2014) Sols-Détermination de la limite de liquidité à l'aide du pénétromètre à cône suédois et de la limite de plasticité. *BNQ-2501-092*, 22.
15. CAN/BNQ (2014) Sols-Détermination de la résistance au cisaillement non drainé et de la sensibilité des sols cohérents à l'aide d'un pénétromètre à cône. *BNQ 2501-110*, 20.
16. MTQ (2016) Essai de consolidation à l'oedomètre. *Standard LC 22-301*, 13.
17. Delage P, Lefebvre G (1984) Study of the structure of a sensitive Champlain clay and its evolution during consolidation. *Can Geotech J* 21: 21–35.
18. LaPierre C, Leroueil S, Locat J (1990) Mercury intrusion and permeability of Louiseville clay. *Can Geotech J* 27: 761–773.

19. La Rochelle P, Leroueil S, Trak B, et al. (1988) Observational approach to membrane and area corrections in triaxial tests. In: Donaghe RT, Chaney RC, Silver ML, editors, *Advanced Triaxial Testing of Soil and Rock*, American Society for Testing and Material, Special Technical Publication 997, Philadelphia, 715–731.
20. ASTM (2011) Standard test method for consolidated undrained compression test for cohesive soils. ASTM D4767-11. *ASTM International*, West Conshohocken, PA, 14.
21. Locat J, St-Gelais D (2014) Nature and Sensitivity Clays from Québec. In: L'Heureux JS, Locat A, Leroueil S, editors. *Advances in Natural and Technological Hazards Research 36 Landslides in sensitive clays From Geosciences to risk management*, Springer, 25–37.
22. Leroueil S, Tavenas F, Le Bihan JP (1983) Propriétés caractéristiques des argiles de l'est du Canada. *Can Geotech J* 20: 681–705.
23. Locat J, Lefebvre G, Ballivy G (1984) Mineralogy, chemistry, and physical properties interrelationships of some sensitive clays from Eastern Canada. *Can Geotech J* 21: 530–540.
24. Locat J (1995) On the development of microstructure in a collapsible soils. NATO Workshop, In: Derbyshire E, editors, *Genesis and Properties of Collapsible Soils*, Kluwer Academic Publishers, 93–128.
25. Bentley SP, Smalley IJ (1978) Inter-particular cementation in Canadian post-glacial clays and the problem of high sensitivity (St > 50). *Sedimentology* 25: 297–307.
26. Demers D, Leroueil S (2002) Evaluation of preconsolidation pressure and the overconsolidation ratio from piezocone tests of clay deposits in Quebec. *Can Geotech J* 39: 174–192.
27. Lunne T, Robertson PK, Powel JJM (1997) *Cone Penetration Testing in Geotechnical Practice*. London: Blackie Academic and Professional.
28. Paniagua P, D'Ignazio M, L'Heureux JS, et al. (2019) CPTU correlations for Norwegian clays: an update. *AIMS Geosci* 5: 82–103.
29. Leroueil S, Hight DW (2003) Behaviour and properties of natural soils and soft rocks. *Charact Eng Prop Nat Soils*, 29–254.
30. La Rochelle P, Lefebvre G (1971) Sampling disturbance in Champlain Sea clays. In: *Sampling of soil and rock*, American Society for Testing and Materials, Special Technical Publication 483, Philadelphia, 143–163.
31. Lefebvre G, Poulin C (1979) A new method of sampling in sensitive clay. *Can Geotech J* 16: 226–233.
32. Leroueil S, Tavenas F, Samson L, et al. (1983) Preconsolidation pressure of Champlain clays. Part II. Laboratory determination. *Can Geotech J* 20: 803–816.
33. Lunne T, Berre T, Andersen KH, et al. (2006) Effects of sample disturbance and consolidation procedures on measured shear strength of soft marine Norwegian clays. *Can Geotech J* 43: 726–750.
34. Locat A, Leroueil S, Bernander S, et al. (2011) Progressive failures in Eastern Canadian and Scandinavian sensitive clays. *Can Geotech J* 48: 1696–1712.
35. Hungr O, Leroueil S, Picarelli L (2013) The Varnes Classification of landslide types, an update. *Landslides* 11: 167–194.
36. Demers D, Robitaille D, Locat P, et al. (2014) Inventory of large landslides in sensitive clay in the province of Québec, Canada: preliminary analysis, In: L'Heureux JS et al., editors. *Advances in Natural and Technological Hazards Research 36 Landslides in sensitive clays From Geosciences to risk management*, Springer, 77–90.

37. Locat A, Demers D, Leroueil S (2016) Spreads in Canadian sensitive clays. In: *Landslides and Engineered Slopes–Experience, Theory and Practice.* In: Aversa S et al., editors, *Proceedings of the 12th International Symposium on Landslides*, Italy, Napoli: Taylor & Francis Group, 1295–1304.
38. Quinn PE, Diederichs MS, Rowe RK, et al. (2011) A new model for large landslides in sensitive clay using a fracture mechanics approach. *Can Geotech J* 48: 1151–1162.
39. Locat A, Jostad HP, Leroueil S (2013) Numerical modeling of progressive failure and its implications for spreads in sensitive clays. *Can Geotech J* 50: 961–978.
40. Locat A, Leroueil S, Fortin A, et al. (2015) The 1994 landslide at Sainte-Monique, Quebec: geotechnical investigation and application of progressive failure analysis. *Can Geotech J* 52: 490–504.
41. Leroueil S, Locat A, Eberhardt E, et al. (2012) Keynote Lecture: Progressive failure in natural and engineering slopes. In: *Landslides and Engineered Slopes: Protecting Society through Improved and Understanding*, Taylor & Francis Group, 31–46.

AIMS Press